Electronic Supplementary Material (ESI) for Journal of Materials Chemistry C.
This journal is © The Royal Society of Chemistry 2023

Electronic supporting information for:

Revealing two chemical strategies to tune bright one- and two-photon excited fluorescence of carbon nanodots

Sebastian G. Mucha,[a] Lucyna Firlej,[a,b] Filip Formalik,[c,d] Jean-Louis Bantignies,[a] Eric Anglaret,[a] Marek Samoć,[e] and Katarzyna Matczyszyn[e,f*]

a. Laboratoire Charles Coulomb, Université de Montpellier (CNRS), Campus Triolet, Place Eugène Bataillon, Montpellier 34095, France.

b. Department of Physics and Astronomy, University of Missouri, Columbia, Missouri 65211, United States.

c. Department of Chemical and Biological Engineering, Northwestern University, Evanston, Illinois 60208, United States.

d. Department of Micro, Nano, and Bioprocess Engineering, Wrocław University of Science and Technology, Wyb. Wyspiańskiego 27, 50-370 Wrocław, Poland.

e. Institute of Advances Materials, Wrocław University of Science and Technology, Wyb. Wyspiańskiego 27, 50-370 Wrocław, Poland.

f. International Institute for Sustainability with Knotted Chiral Meta Matter (WPI-SKCM2), Hiroshima University, Higashihiroshima, Hiroshima 739-8526, Japan.

Contents:

Fabrication of PG CNDs: synthesis routines

Figure S1. The simplified scheme of the fabrication routes leading to individual PG CNDs.

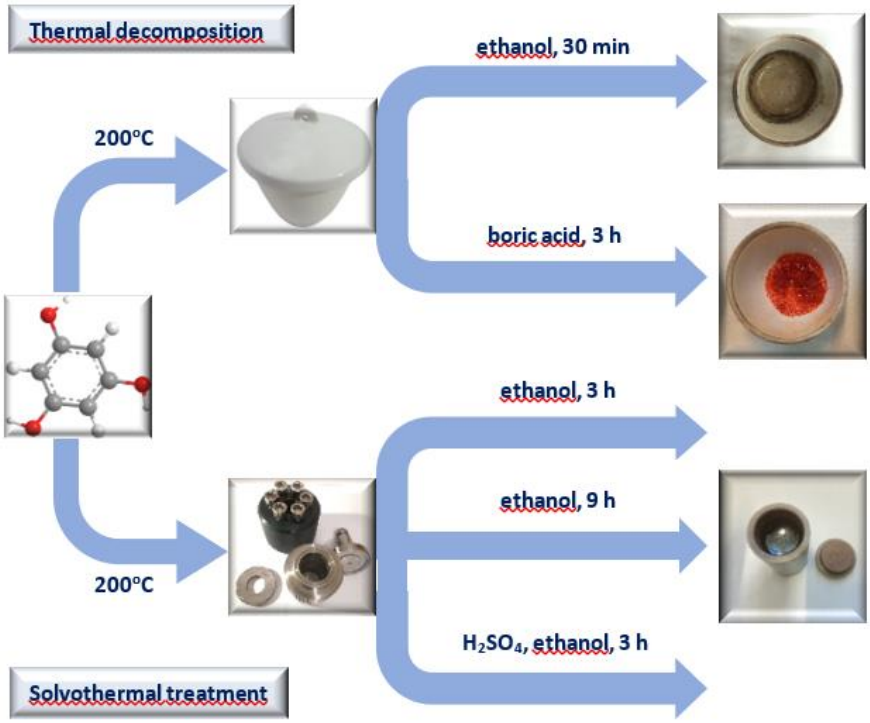

Fabrication of PG CNDs: neutralization of acid-catalyzed reaction mixture

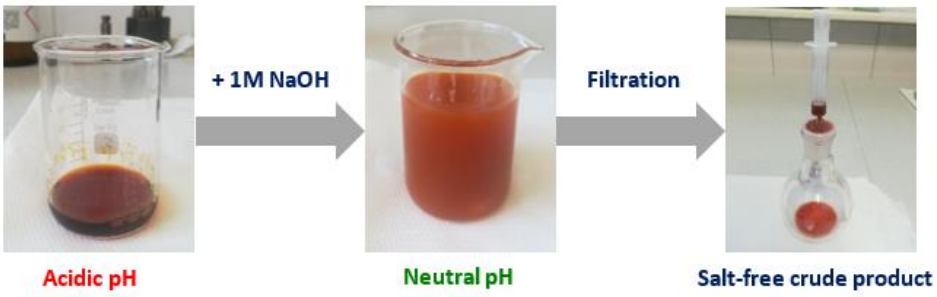

Figure S2. The schematic depiction of the neutralization of YELLOW CNDs (crude product) derived from the acid-mediated synthesis.

Purification of PG CNDs

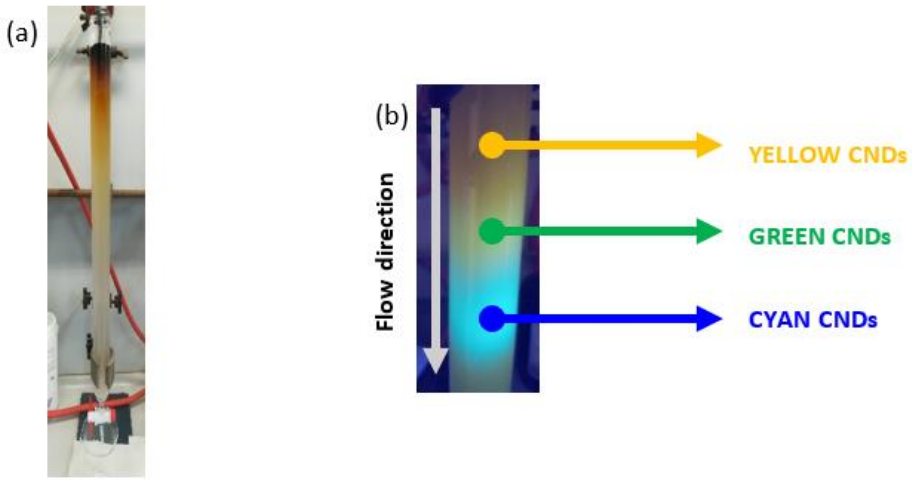

Figure S3. The silica column chromatography (SCC) system purifying a reaction mixture of **CYAN** CNDs (a). The separation of mixture of three kinds of PG CNDs on the same experimental conditions (b).

HR-TEM imaging

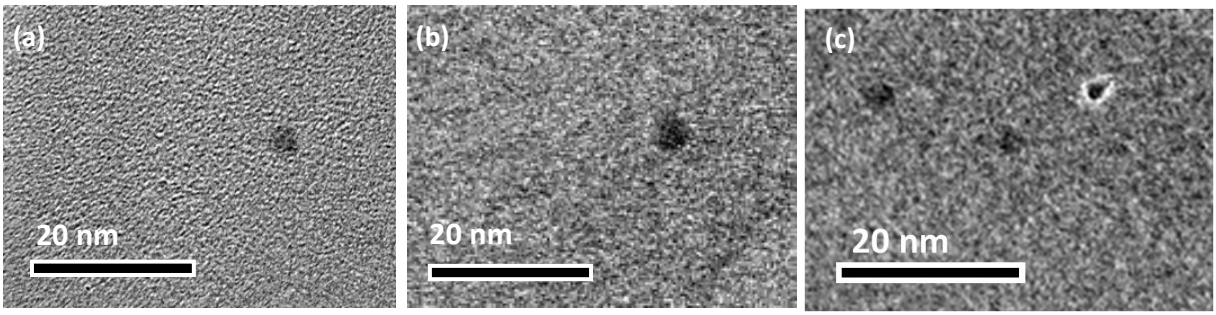

Figure S4. The HR-TEM images of representative **CYAN** CNDs.

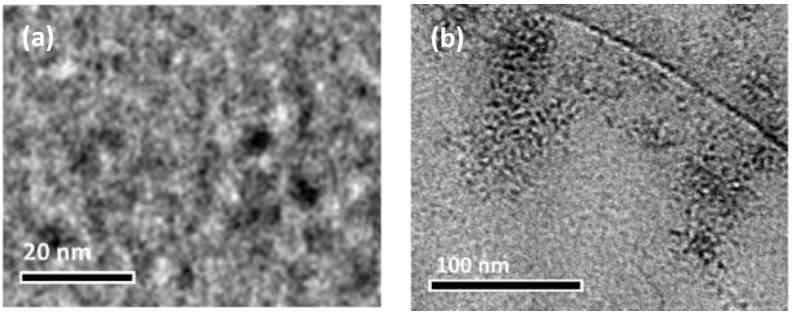

Figure S5. The HR-TEM images of representative **GREEN** CNDs.

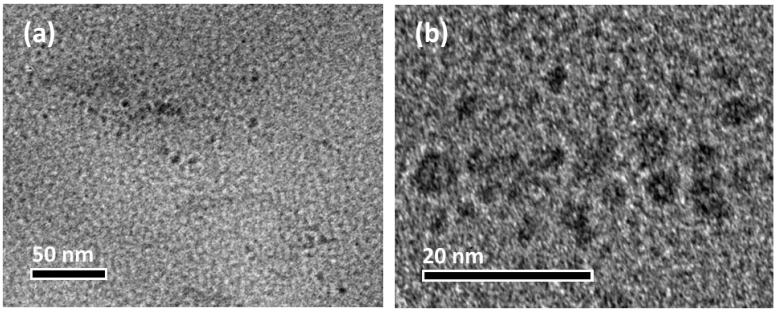

Figure S6. The HR-TEM images of representative **YELLOW** CNDs.

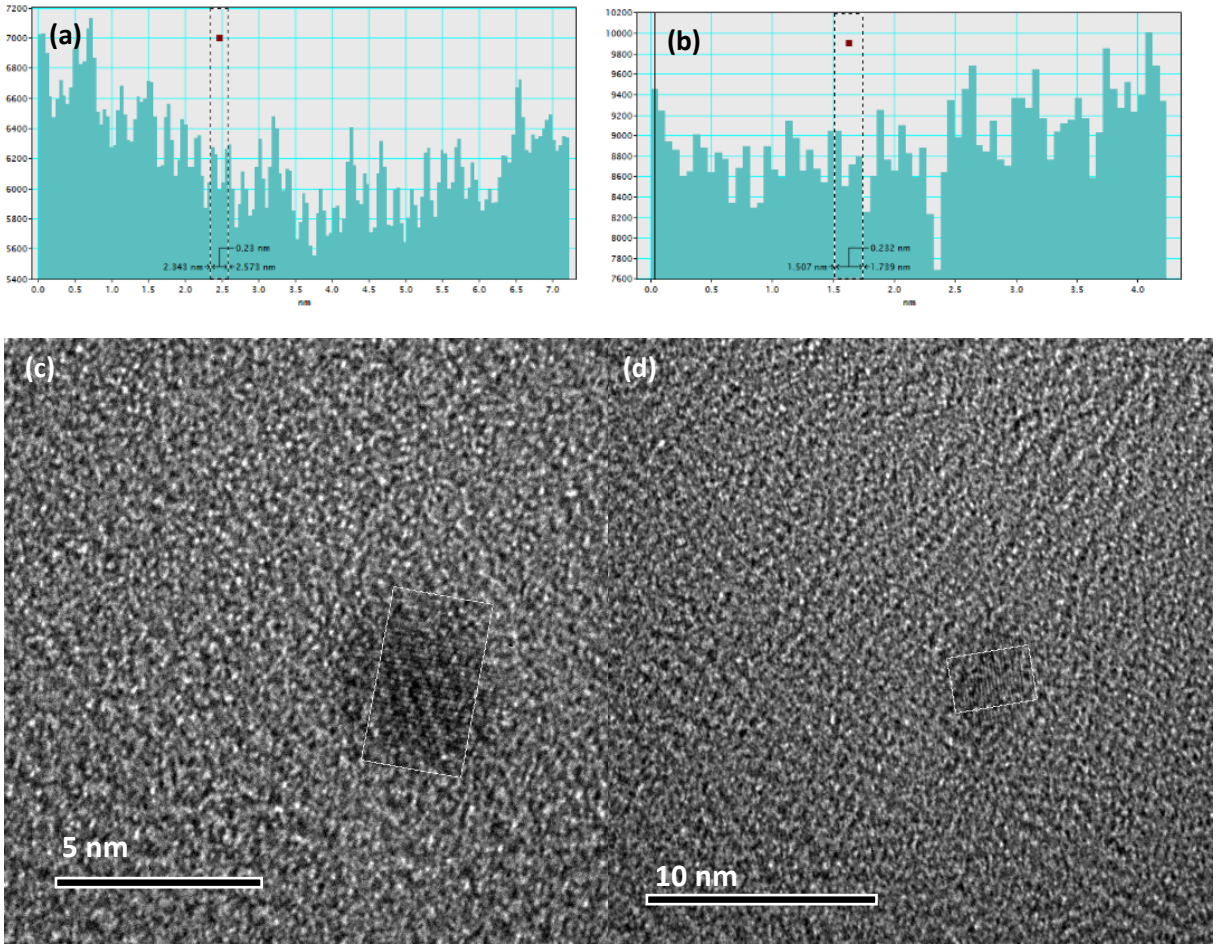

Figure S7. The HR-TEM images of single PG CNDs (a-b) with their corresponding pixel intensity profiles (c-d).

STEM-EDX spectra

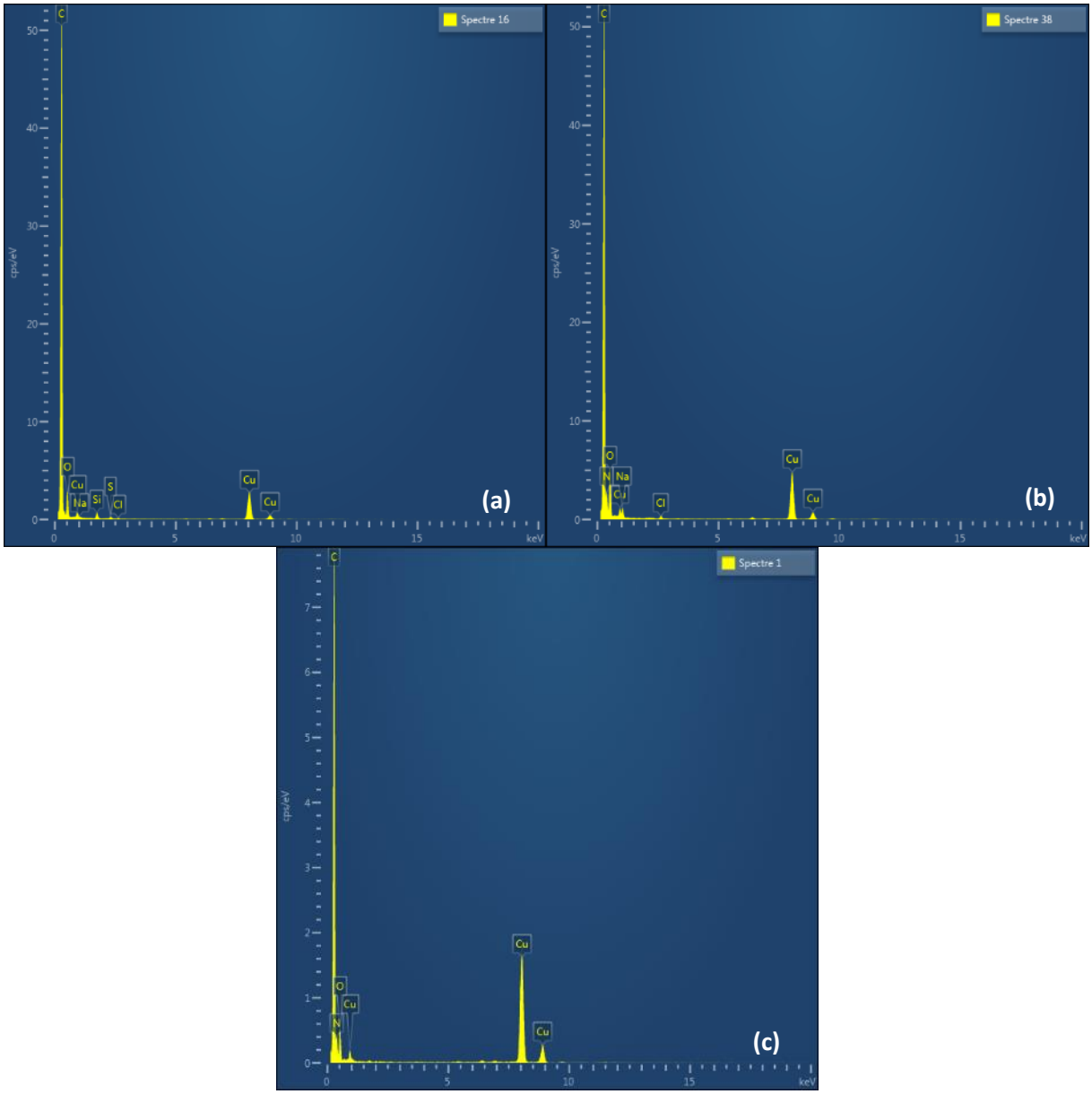

Figure S8. The EDX-STEM profiles of PG CNDs. The individual components are indicated.

XPS spectra

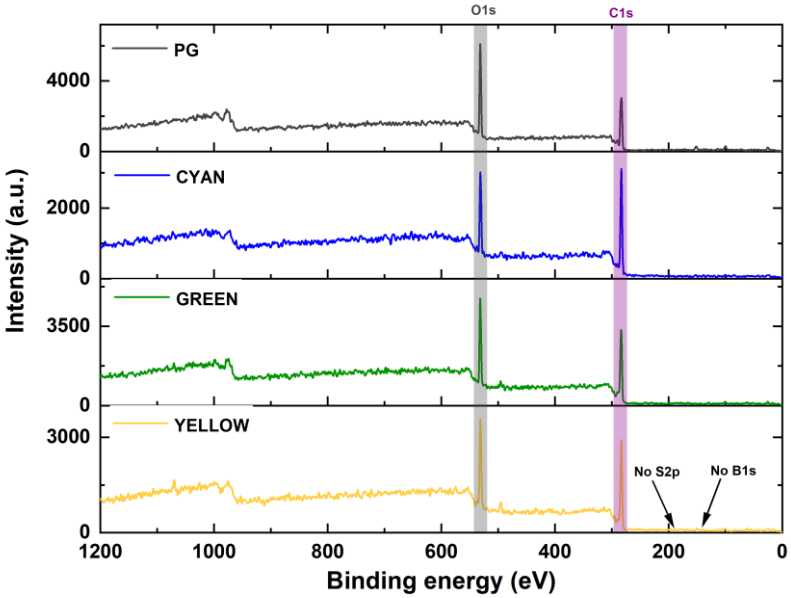

Figure S9. The XPS surveys of the PG and PG CNDs. Both crucial peaks (**O1s** and **C1s**) are indicated. Note that all CNDs are free of catalyst impurities.

General NMR spectra

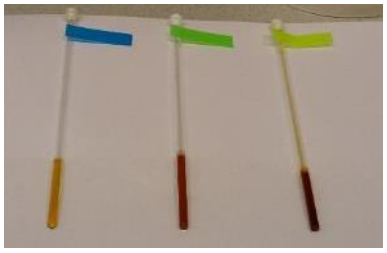

Figure S10. The d_4-methanol dispersions of PG CNDs in the NMR tubes: **CYAN**, **GREEN**, and **YELLOW**.

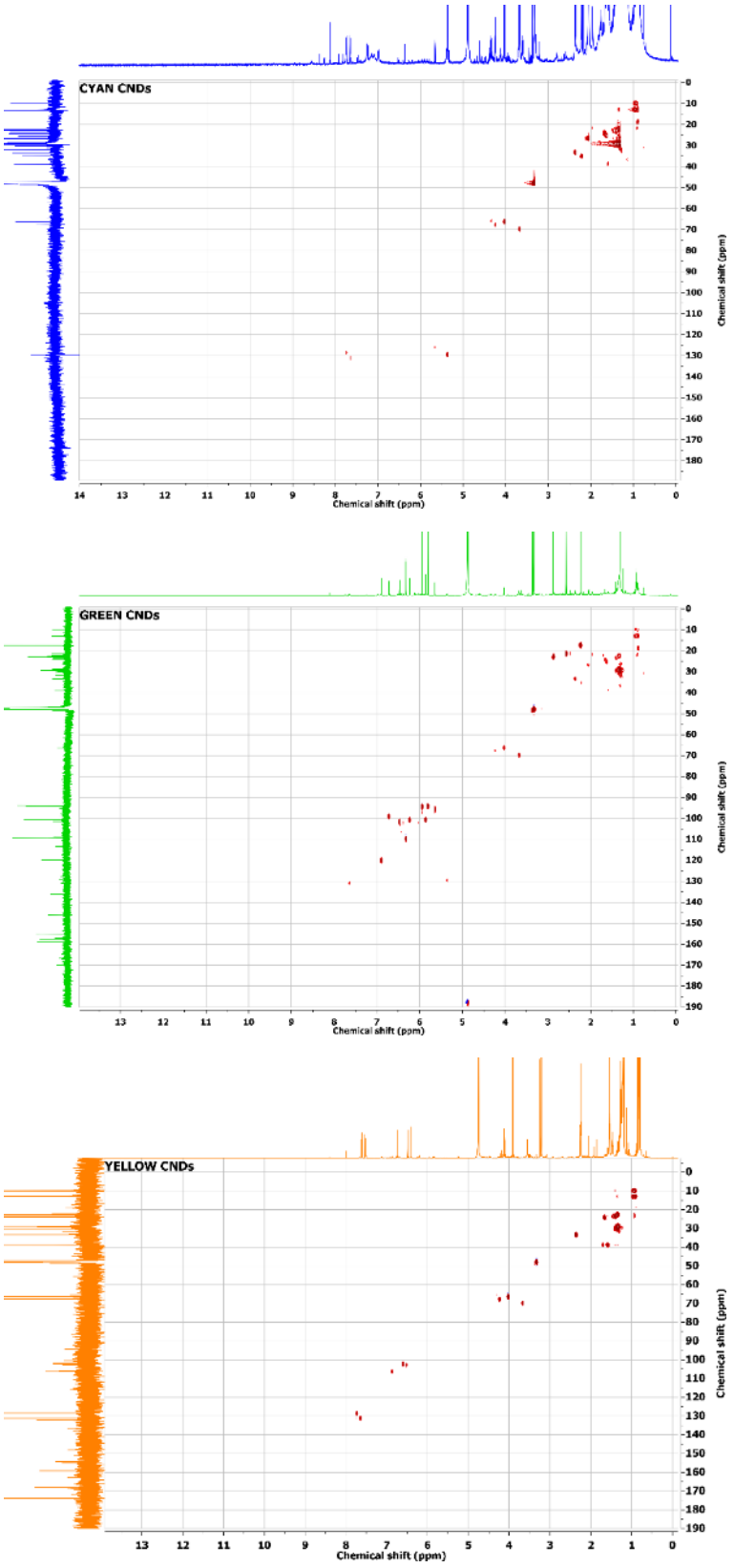

Figure S11. The HSQC NMR spectra of PG CNDs dispersed in d_4-methanol.

NMR spectra: downfield region

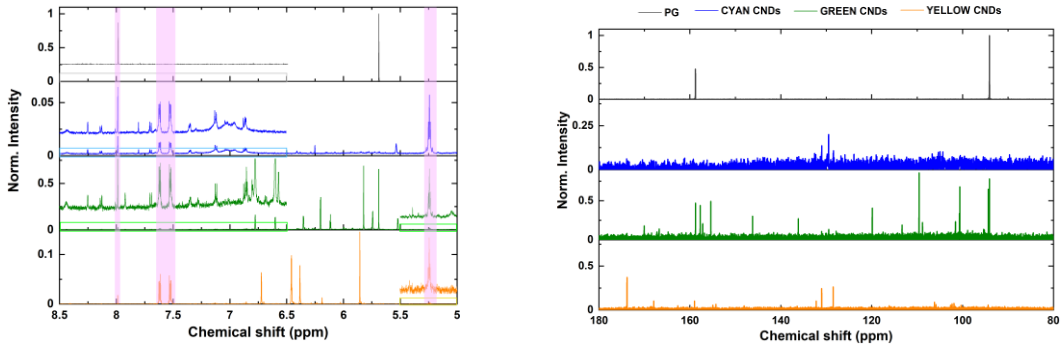

Figure S12. The ^{1}H (a) and ^{13}C NMR (b) spectra of PG and PG CNDs in the downfield region. Some NMR signals are zoomed, as highlighted with coloured frames. The crucial common signals are marked with violet areas.

NMR spectra: upfield region

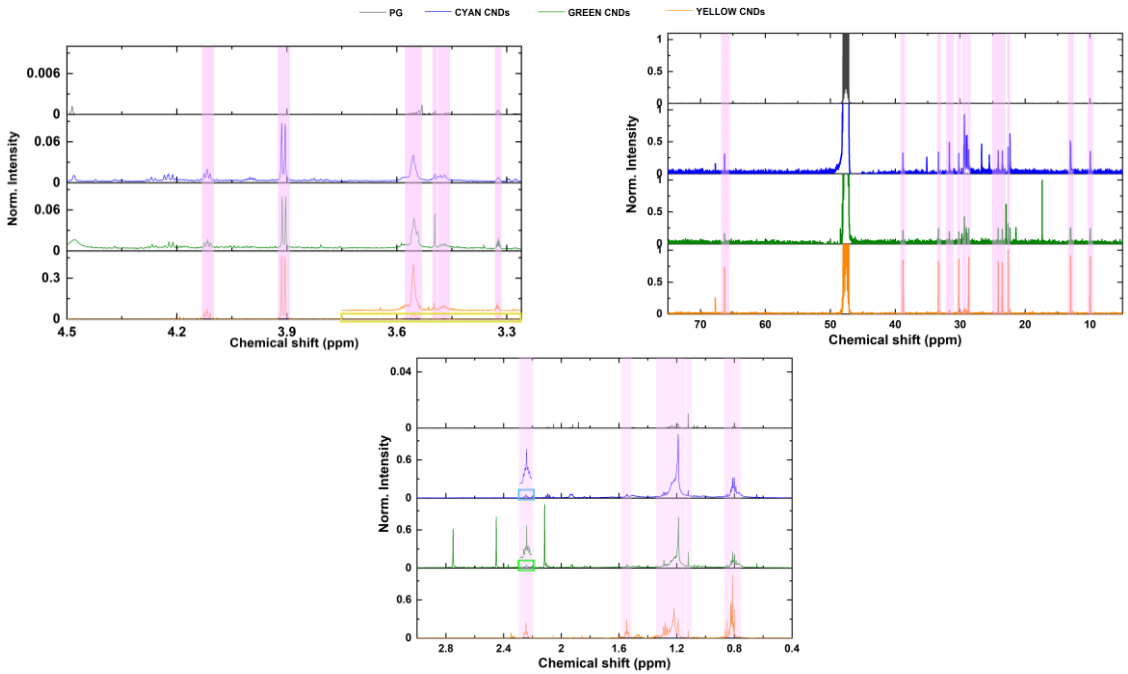

Figure S13. The ^{1}H (a) and ^{13}C NMR (b, c) spectra of PG and PG CNDs in the upfield region. Some NMR signals are zoomed, as highlighted with coloured frames. The crucial common signals are marked with violet areas.

IR spectra of PG precursor: theoretical studies

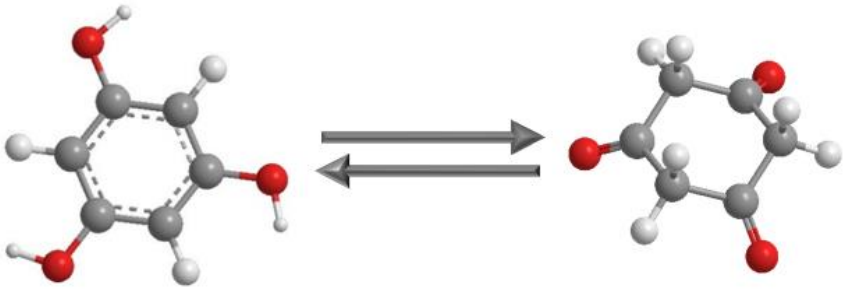

Figure S14. The keto-enol tautomerism of a phloroglucinol (PG) molecule. In the solution, the particular form of PG depends on the donor-acceptor nature of the solvent in the formation of the hydrogen-bonding network with the solute:

- **Enol form:** polar aprotic solvents (*e.g.* d_6-DMSO) - solvents with the great ability to **accept** hydrogen from another molecule *via* the hydrogen bond;
- **Keto form:** protic solvents (*e.g.* methanol) - solvents able to **donate** (share) hydrogen to another molecule *via* the hydrogen bond;[1-2]

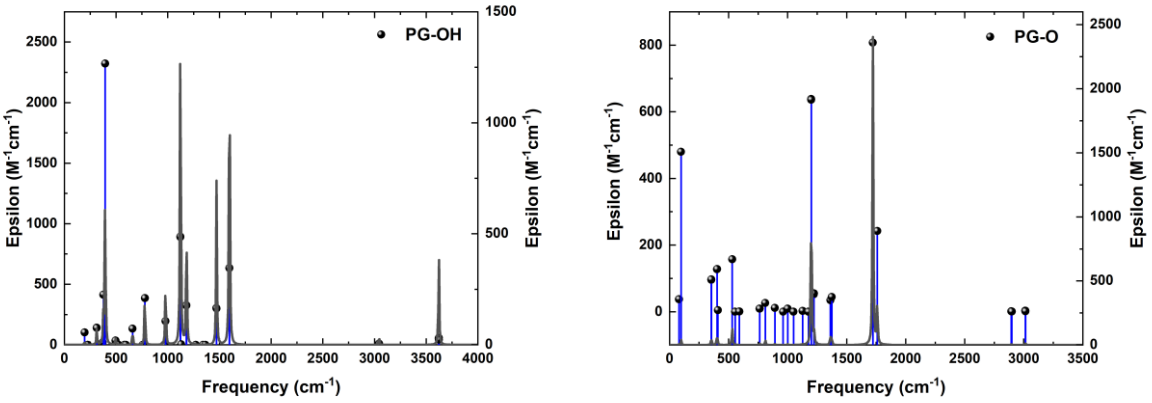

Figure S15. The IR spectra of a PG molecule in the enol (PG-OH; a) and ketone (PG-O; b) form. The calculated vibration signals (presented as point–line combinations) are fitted with the Lorentzian function (grey curves). The width of each Lorentzian peak is 4 cm^{-1}.

FTIR spectroscopy: experimental assays

Figure S16. The analytes in KBr pellets (a) and the sample chamber in the IR spectrometer operating in the transmission mode (b).

Figure S17. The YELLOW CNDs in the d_6-DMSO suspension (a), the construction of the CaF_2 liquid cell (b-c), and the view of the sample chamber in the IR spectrometer working in the transmission mode (d).

Figure S18. The sample chamber in the IR spectrometer operating in the attenuated total reflectance mode.

IR spectra of PG precursor: theoretical *vs.* experimental studies

Table S1. The theoretical and experimental infrared characteristics of PG molecules (part I).

Peak Position (cm^{-1})				Band assignments
Theoretical		Experimental		
PG-OH[a]	PG-O[b]	ATR[c]	TR[d]	
-	80,	-	-	ρ ring vibration
-	98	-	-	ρ ring vibration, ρCO (ketone)
-	-	62, 109, 122, 152	-	Hydrogen bond vibrations*
196	-	-	-	ρ ring vibration$_{symmetrical}$ **(1,3,5-trisubstituted)**
226-227	-	230, 236	-	ρ ring vibration
-	-	252	-	-
-	-	270	-	-
313	-	-	-	δCO (phenol)
-	354	-	-	ν ring vibration
371, 377****	-	363	-	ρOH, ρCH$_{aromatic}$
394****	-	382	-	ρOH$_{symmetrical}$ **(1,3,5-trisubstituted)**
-	402, 409	-	-	δCO, δCH$_{methylene}$
495	-	*Included in stronger peak***	-	δC=C$_{aromatic}$
524	-	521	521	δCO$_{symmetrical}$ (phenol) **(1,3,5-trisubstituted)**
-	530	-	-	ρCO (ketone), ν ring vibration
-	555	-	-	δCO (ketone), ν ring vibration
582	-	582	582	νring$_{symmetrical}$ **(1,3,5-trisubstituted)**
-	591	-	-	Ring breathing (cycloalkane)
596	-	600	600	ρOH, ρCH$_{aromatic}$, ρring vibration
-	-	647	-	-
660	-	664	675	ρCH$_{aromatic}$ and CO (phenol) **(1,3,5-trisubstituted)**
758	-	-	-	ρCH$_{aromatic}$
-	763	-	-	ρC- C$_{methylene}$, δCH$_{methylene}$
779	-	799	801	ρCH$_{aromatic,\ symmetrical}$ **(1,3,5-trisubstituted)**
-	811	812	815	νC-C$_{methylene}$, ρCH$_{methylene}$
-	-	839	840	-

Table S2. The theoretical and experimental infrared characteristics of PG molecules (part II).

Peak Position (cm^{-1})				Band assignments
Theoretical		Experimental		
PG-OH[a]	PG-O[b]	ATR[c]	TR[d]	
-	892	-	-	v $ring_{symmetrical}$
-	962	*Included in stronger peak***	*Included in stronger peak***	δC-$C_{methylene}$, δ$CH_{methylene}$, δC=O (ketone)
966	-	-	-	v $ring_{symmetrical}$ **(1,3,5-trisubstituted)**
979****	-	995*	999, 1007*	vring, δ$CH_{aromatic}$, δ$OH_{aromatic}$, vCO (phenol)
-	1001			δC-$C_{methylene}$, δ$CH_{methylene}$, δC=O (ketone)
-	1050	-	-	vC-$C_{methylene}$, ρ$CH_{methylene}$, δC=O (ketone)
-	1127	1150	1156	ρ$CH_{methylene}$
1122, 1130****	-			vring, δ$CH_{aromatic}$, δ$OH_{aromatic}$, vCO (phenol) **(1,3,5-trisubstituted)**
-	1176	-	-	ρ$CH_{methylene}$
1181	-	1190	1188	vring, δ$CH_{aromatic}$, δ$OH_{aromatic}$, vCO (phenol)
-	1200	1209	-	vC-$C_{methylene}$, ρ$CH_{methylene}$, δC=O (ketone)
-	1223	-	-	vC-$C_{methylene}$, ρ$CH_{methylene}$,
1272	-	1281	*Included in stronger peak***	δ$CH_{aromatic}$, δOH, vC=$C_{aromatic}$ (semicircle),
-	-	1304	1315	-
1340	-	1330	1336	v$CO_{aromatic}$
1364	-	1351, 1369	*Included in stronger peak***	vC=$C_{aromatic}$ (semicircle), δ$CH_{aromatic}$, δOH
-	1362, 1374	*Included in stronger peak***	*Included in stronger peak*	δ$CH_{methylene}$
-	-	1407, 1433, 1439	1411, 1416, 1428	-
1471****	-	1504****	1508****	vC=$C_{aromatic}$ (semicircle), δ$CH_{aromatic}$, δOH
1596-1597****	-	1620****	1626****	vC=$C_{aromatic}$ (quadrant), δ$CH_{aromatic}$, δOH
-	1722	-	-	vC=O (ketone)
-	1759	1760 *(very weak)****	1760 *(very weak)****	vC=$O_{symmetrical}$ (ketone)
-	2895-2900	-	-	v$CH_{methylene}$
-	3013-3015	-	-	
3044-3045	-	3071	3073	v$CH_{aromatic}$
3620-3623****	-	3206****	-	vOH

Labelling (it is also dedicated to **Tables S1**): ν - stretching; δ – in-plane bending; ρ – out-of-plane bending;

a – the enol form of a PG molecule (see tautomerism equation in **Figure S14**);

b – the ketone form of a PG molecule (see tautomerism equation in **Figure S14**);

c – the experimental results of the attenuation total-reflectance FTIR measurements;

d - the experimental results of the transmission FTIR measurements (samples are trapped in the KBr pellet);

e – the experimental results of the transmission FTIR assays (samples are dispersed in d_6-DMSO); Note: those results were considered above 1200 cm^{-1};

* - the hydrogen bond vibrations of phenols are expected in the range of 80-200 cm^{-1};

** - those IR signals are confirmed; their precise position cannot be identified – they are embedded into stronger IR components close to them;

*** - those IR components have very low intensity as compared to other signals;

**** - the position of those IR signals is strongly affected by the hydrogen bonding network;

Typical IR signals of the PG molecules are **marked**.

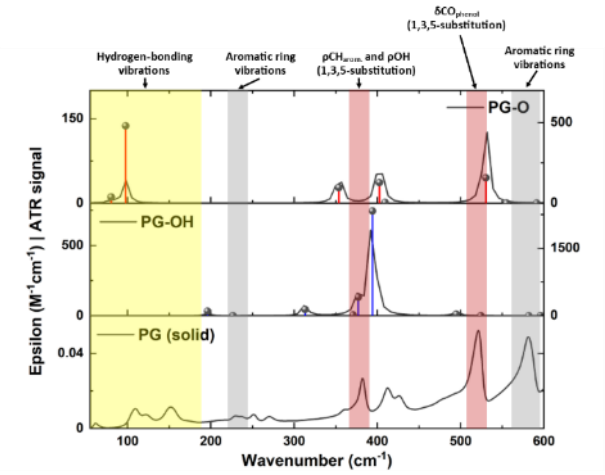

Figure S19. The calculated IR spectra of both forms of a PG molecule (PG-O and PG-OH) and the experimental ATR-FTIR spectrum (PG (solid)) in the FIR region. The signatures of the most essential chemical groups are indicated.

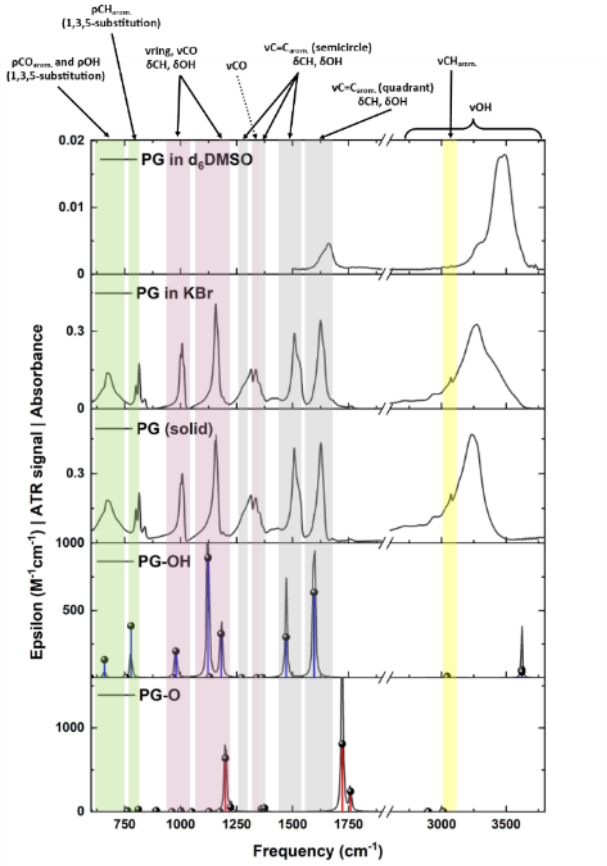

Figure S20. The calculated IR spectra of both forms of a PG molecule (PG-O and PG-OH) and the experimental FTIR spectra in the MIR region. The experimental results are named relying on the chemical environment of each sample (*i.e.* KBr, d_6-DMSO, or pure solid-state form). The signatures of the most essential chemical groups are indicated.

FTIR spectra of PG and PG CNDs

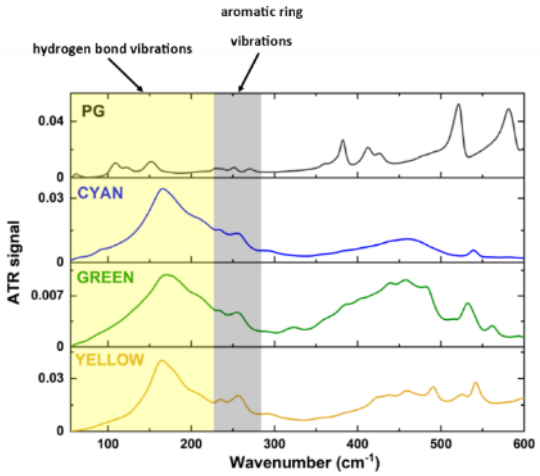

Figure S21. The FTIR spectra of PG molecules and PG CNDs in the far-infrared range. The most crucial vibration modes are indicated.

Raman spectra of PG and PG CNDs

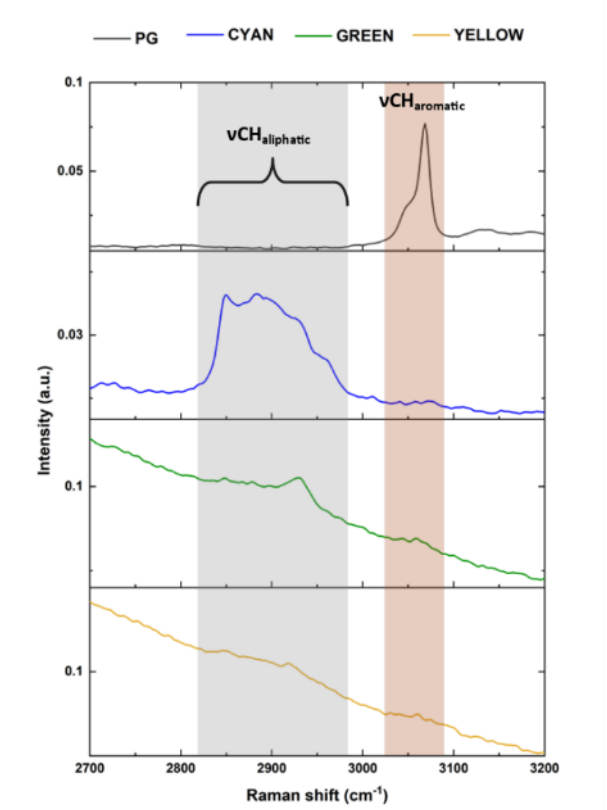

Figure S22. The Raman spectra of PG and PG CNDs in the high-frequency range. Two crucial Raman signals are marked.

Table S3. The Raman characteristics of PG molecules and PG CNDs.

Raman shift (cm^{-1})*				Band assignments
PG	**CYAN**	**GREEN**	**YELLOW**	
3069	-	-	-	$\nu CH_{aromatic}$
-	2851, 2883, 2928	2849, 2880, 2930	2853, 2878, 2918	$\nu CH_{aliphatic}$
1592, 1611, 1638	1592, 1608, 1642	1589-1634	1592-1618	$\nu C{=}C_{aromatic}$ (quadrant mode)
1498, 1532	-**	*minor****	1518, 1535	$\nu C{=}C_{aromatic}$ (furan)
-	1441	1441, 1461	1430, 1441	$\delta CH_{aliphatic}$ (scissoring mode)
1220, 1294, 1310, 1361	1297, 1354	1309, 1342, 1360, 1378	1224, 1297, 1322, 1342, 1378	$\nu C{=}C_{aromatic}$ (semicircle mode)
-	*minor*	*minor*	1196	$\nu COC_{aliphatic}$ (cyclic ethers) / $\delta CH_{aromatic}$
1156	*minor*	*minor*	1167	$\delta CH_{aromatic}$
-	1051, 1121	1029	*minor*	$\nu CCC_{aliphatic}$ and $\nu CCO_{aliphatic}$
997, 1009	-	-	1005	$\delta CH_{aromatic}$

Labelling: ν - stretching; δ – in-plane bending;

* - Broad Raman bands of PG CNDs (the C=C aromatic stretching) are more complex than their maxima may indicate; some Raman components are included with no showing precise maxima;

** - those signals cannot be identified;

*** - the signals can be confirmed; however, it is difficult to identify their maxima;

XPS spectra: deconvolution results

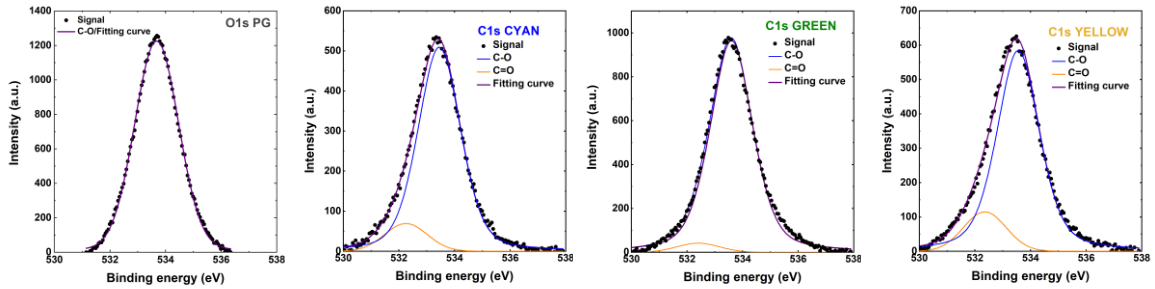

Figure S23. The high-resolution O1s peaks of the PG and PG CNDs with their Gaussian deconvolution results.

Table S4. The Gaussian deconvolution results of the C1s peaks.

Band assignment	Contribution (%)			
	PG	CYAN	GREEN	YELLOW
Non-polar carbon groups	57%	70%	60%	55%
Polar carbon groups	43%	30%	40%	45%

Table S5. The peak ratio according to the deconvolution analysis of the C1s peaks.

Band assignment	Ratio			
	PG	CYAN	GREEN	YELLOW
C=C:C-C	-	1.4	2.1	2.5
C-O:C=C	0.8	0.6	0.7	0.9
C-O:C-C	-	0.8	1.4	2.2
Polar C:Non-polar C	0.8	0.4	0.7	0.8

UV-Vis extinction, one-photon excitation, and one-photon excited emission spectra

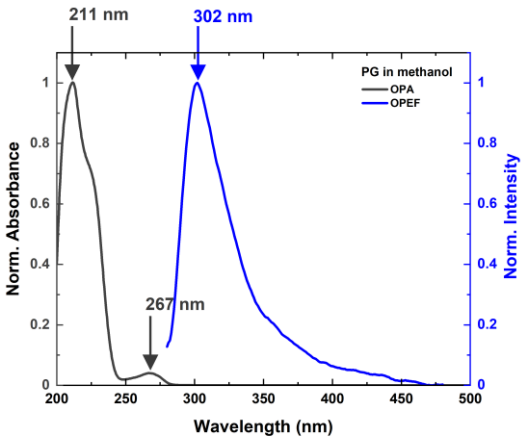

Figure S24. The normalized one-photon absorption and one-photon excited emission spectra of PG molecules in methanol solution.

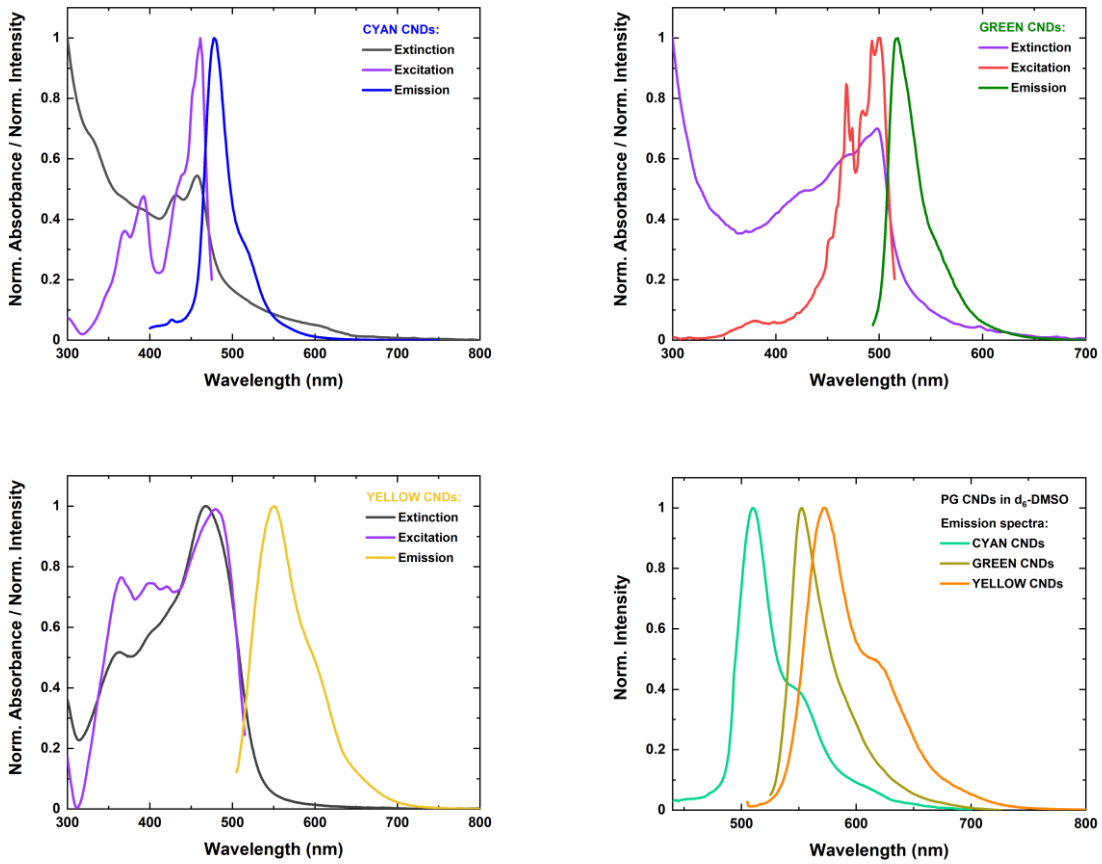

Figure S25. The normalized extinction, one-photon excitation, and one-photon excited emission spectra of PG CNDs in methanolic suspensions (a-c). The normalized emission spectra of PG CNDs in d_6-DMSO dispersions (d).

Optical bandgap estimation

To determine the optical bandgap energy of PG CNDs, the Tauc relation were followed:[3-4]

$$\mathbf{Ah\nu \sim (h\nu - \Delta E)^2} \textit{ (equation 1)}$$

where **A** is absorbance (assuming that it is proportional to the absorption coefficient (α [cm^{-1}]) for the considered concentrations of CNDs:); **hν** denotes the photon energy (*i.e.* energy recalculated from the wavelength value of the extinction spectrum) (eV); **ΔE** is the optical bandgap energy (eV); the index "2" indicates that the indirect electronic transitions are described by the bandgap energy;

Hence, the relation was plotted as **$(Ah\nu)^{1/2}$ *vs.* hν** in the range of the long-wavelength absorption peak and fitted with the linear function as shown in **Figure S26**; the fitting line was then extrapolated and the ΔE value was extracted (for y=0);

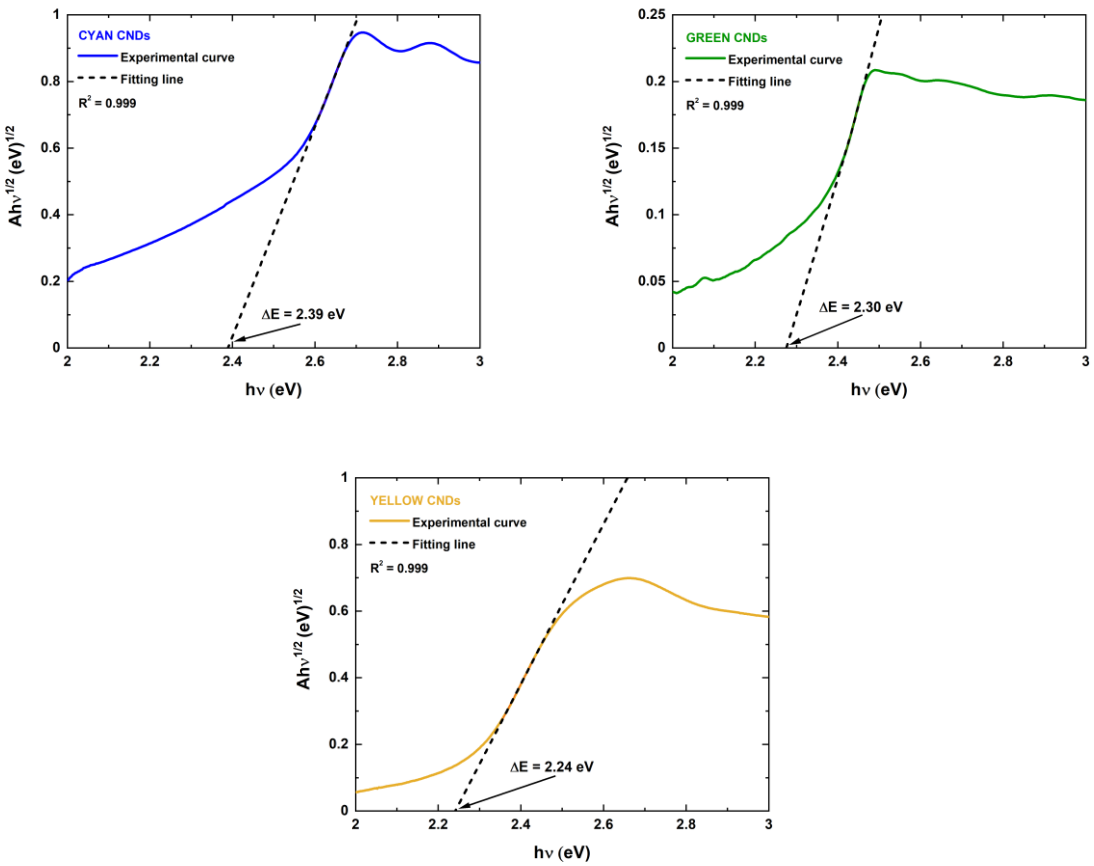

Figure S26. The $(Ah\nu)^{1/2}$ *vs.* hν relation with the estimated bandgap energy values (ΔE) for **CYAN**, **GREEN**, and **YELLOW** CNDs in methanol dispersions.

The above studies do not include the quantitative analysis of the intraband region (*i.e.* hν < ΔE), as the respective intraband states are considered generally in the section: *Fluorescence mechanism*.

One-photon excitation-emission maps

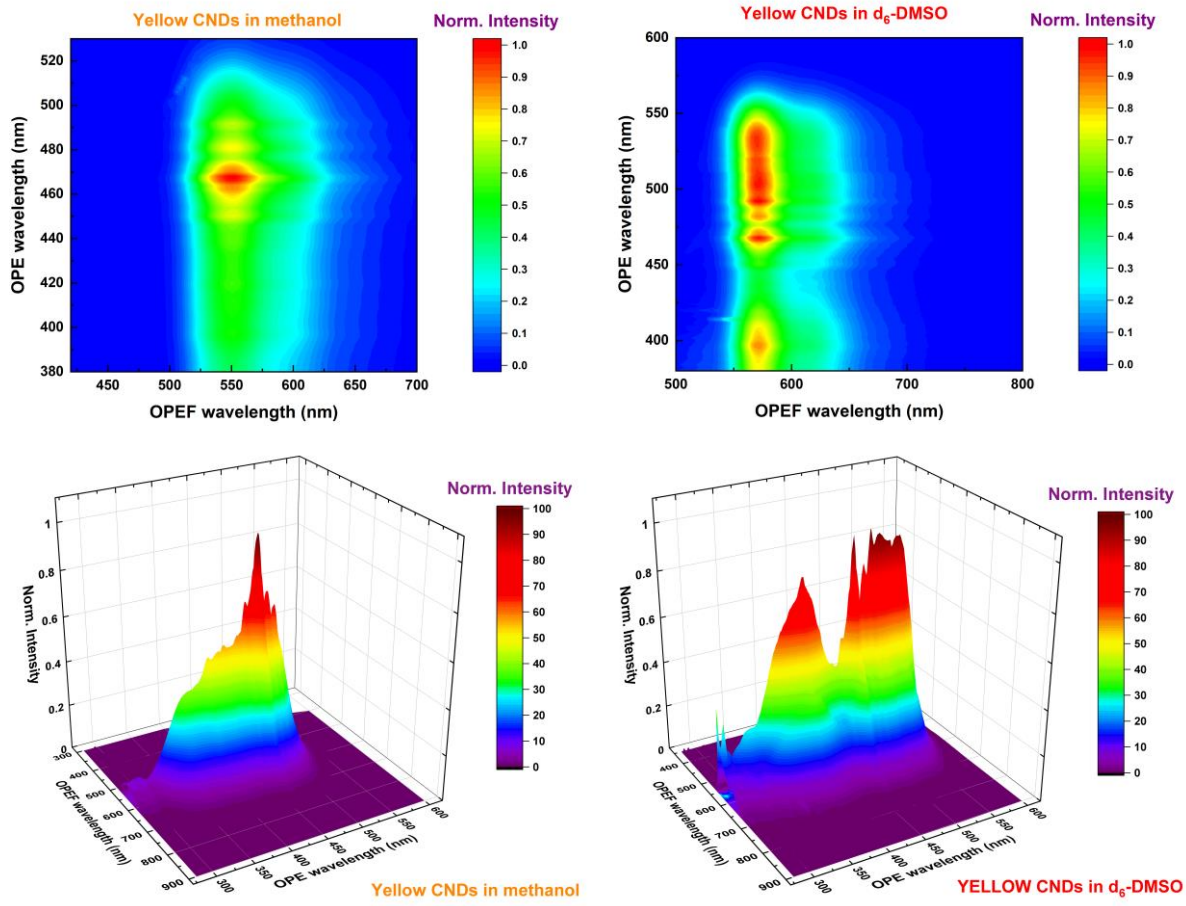

Figure S27. The one-photon excitation-emission maps and three-dimensional spectrum of YELLOW CNDs in d_6-DMSO and methanol dispersions.

Determination of absolute fluorescence quantum yields

The absolute fluorescence quantum yields (FQYs) have been estimated, taking into an account of the excitation signals and emission region in the presence of pure methanol and its dispersions of PG CNDs, following the formula:

$$\mathbf{FQY} = \frac{\mathbf{S_2 - S_3}}{\mathbf{S_0 - S_1}} \cdot \mathbf{100\%} \textit{ (equation 2)}$$

where **FQY** is the fluorescence quantum yield (%), $\mathbf{S_2}$ is the integrated PL intensity of a dispersion of CNDs (a.u.), $\mathbf{S_0}$ and $\mathbf{S_1}$ denote the integrated intensity of an excitation light in the absence and presence of a solute (a.u.), respectively, $\mathbf{S_3}$ is the background in the emission region (a.u.);

Table S6. The fluorescence quantum yield values of PG CNDs.

FQY±SD (%)		
Solvent	methanol	d_6-DMSO
CYAN	61.8±9.9	67.9±2.6
GREEN	29.7±2.9	51.1±2.5
YELLOW	25.2±0.4	44.9±1.9

Fluorescence decay profiles

The fluorescence decays have been judiciously fitted with mono- (*equation 3*) or bi-exponential (*equation 4*) formula as follows:

$$\mathbf{I(t) = A_1 \cdot exp\left(-\frac{t}{\tau_1}\right)} \quad \textit{(equation 3)}$$

$$\mathbf{I(t) = A_1 \cdot exp\left(-\frac{t}{\tau_1}\right) + A_2 \cdot exp\left(-\frac{t}{\tau_2}\right)} \quad \textit{(equation 4)}$$

where **I(t)** is fluorescence intensity (a.u.), **t** is time (ns), τ_1 and τ_2, denote lifetime components, and A_1 and A_2 correspond to their relative decays;

In the case of the bi-exponential decay profile, the weighted averaged fluorescence lifetimes were calculated using a formula:

$$\langle \tau \rangle = \frac{\sum A_i \cdot \tau_i^2}{\sum A_i \cdot \tau_i} \quad \textit{(equation 5)}$$

where τ_i denotes the lifetime *i*-component (ns), A_i is a relevant normalized amplitude, and **<τ>** corresponds to the weighted average lifetime (ns);

When combining fluorescence lifetimes and quantum yields, the rate constants of radiative and non-radiative transitions can be estimated:

$$\mathbf{FQY} = \frac{\mathbf{k_r}}{\mathbf{k_r + k_{nr}}} \qquad \langle \boldsymbol{\tau} \rangle = \frac{\mathbf{1}}{\mathbf{k_r + k_{nr}}} \quad \textit{(equations 6-7)}$$

where **<τ>** denotes the weighted average fluorescence decay time (ns), **FQY** denotes the absolute fluorescence efficiency, k_r and k_{nr} are the rate constants of radiative and non-radiative transitions (ns^{-1}), respectively,

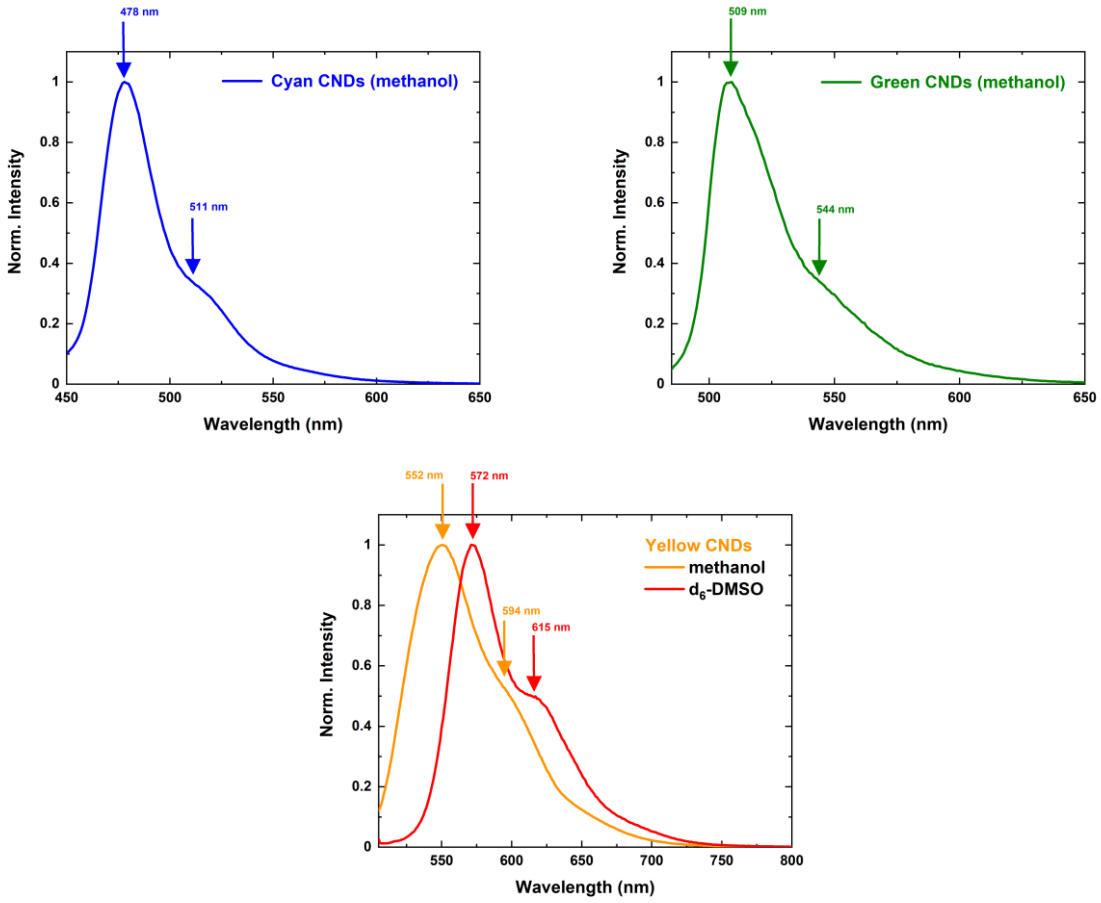

Figure S28. The OPEF spectra of particular PG CNDs' fractions with arrows indicating the emission wavelengths for recording the fluorescence decays.

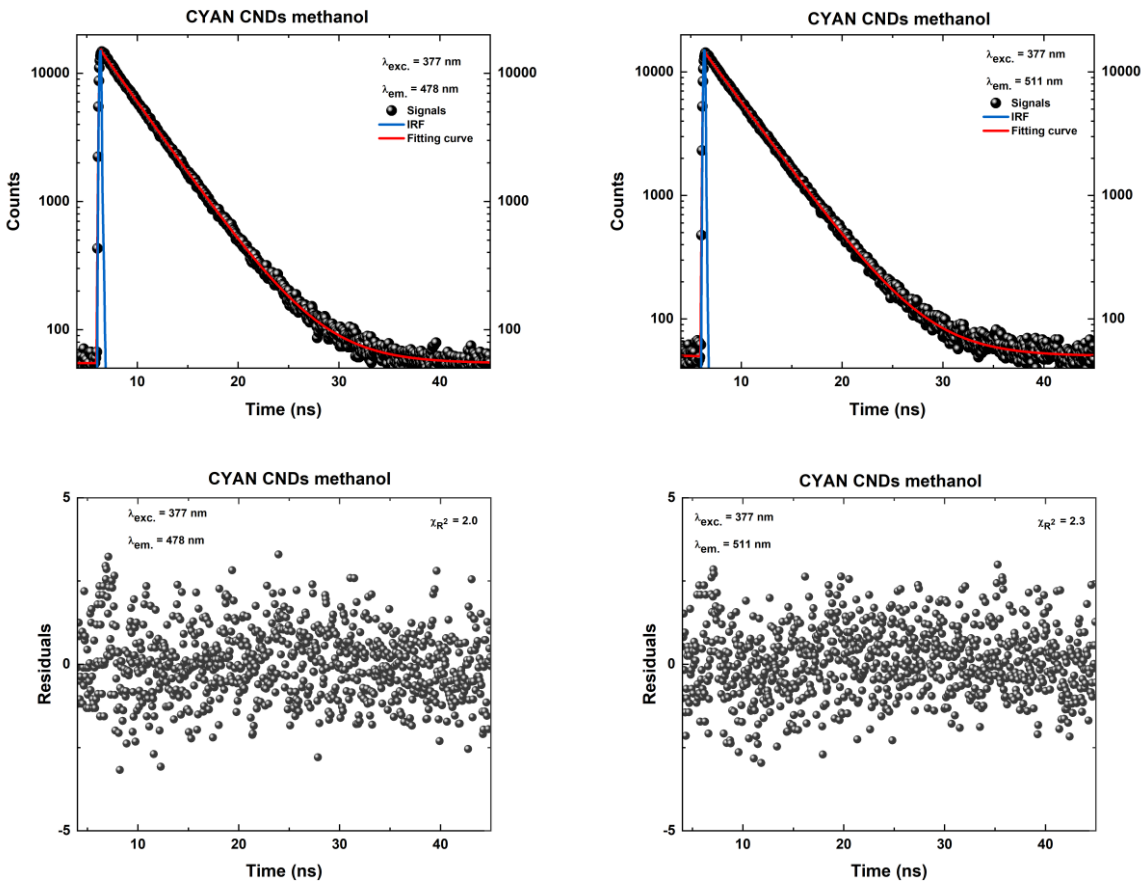

Figure S29. The fluorescence decay profiles of **CYAN** CNDs in methanol and their residual plots recorded at 478 nm and 511 nm, respectively.

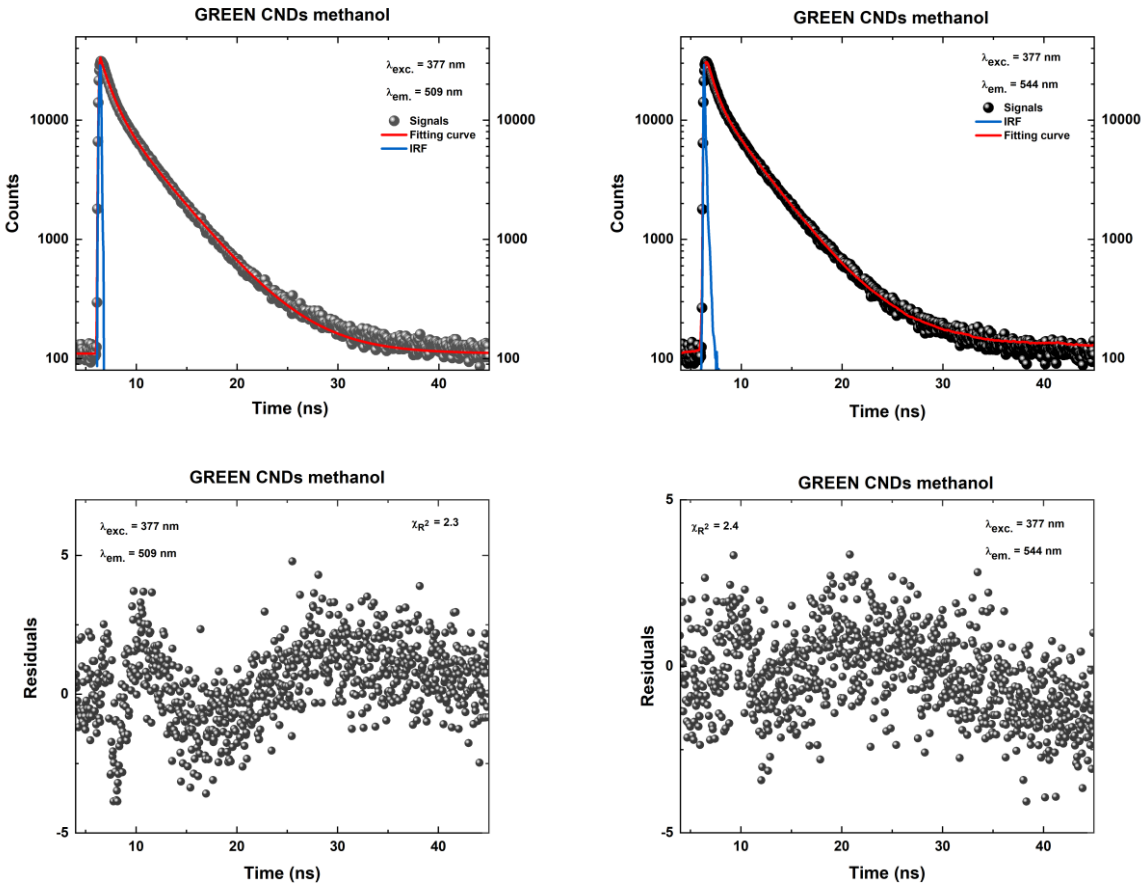

Figure S30. The fluorescence decay profiles of **GREEN** CNDs in methanol and their residual plots recorded at 509 nm and 544 nm, respectively.

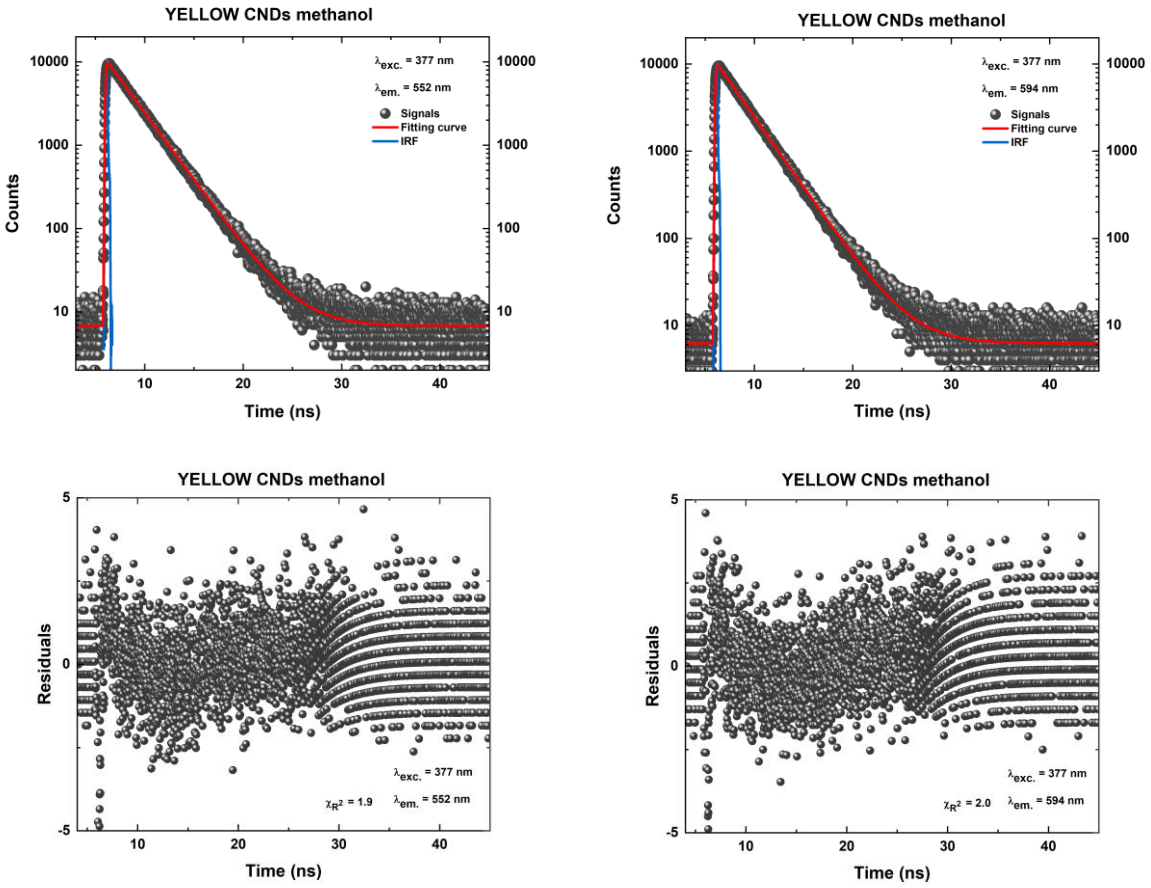

Figure S31. The fluorescence decay profiles of YELLOW CNDs in methanol and their residual plots recorded at 552 nm and 594 nm, respectively.

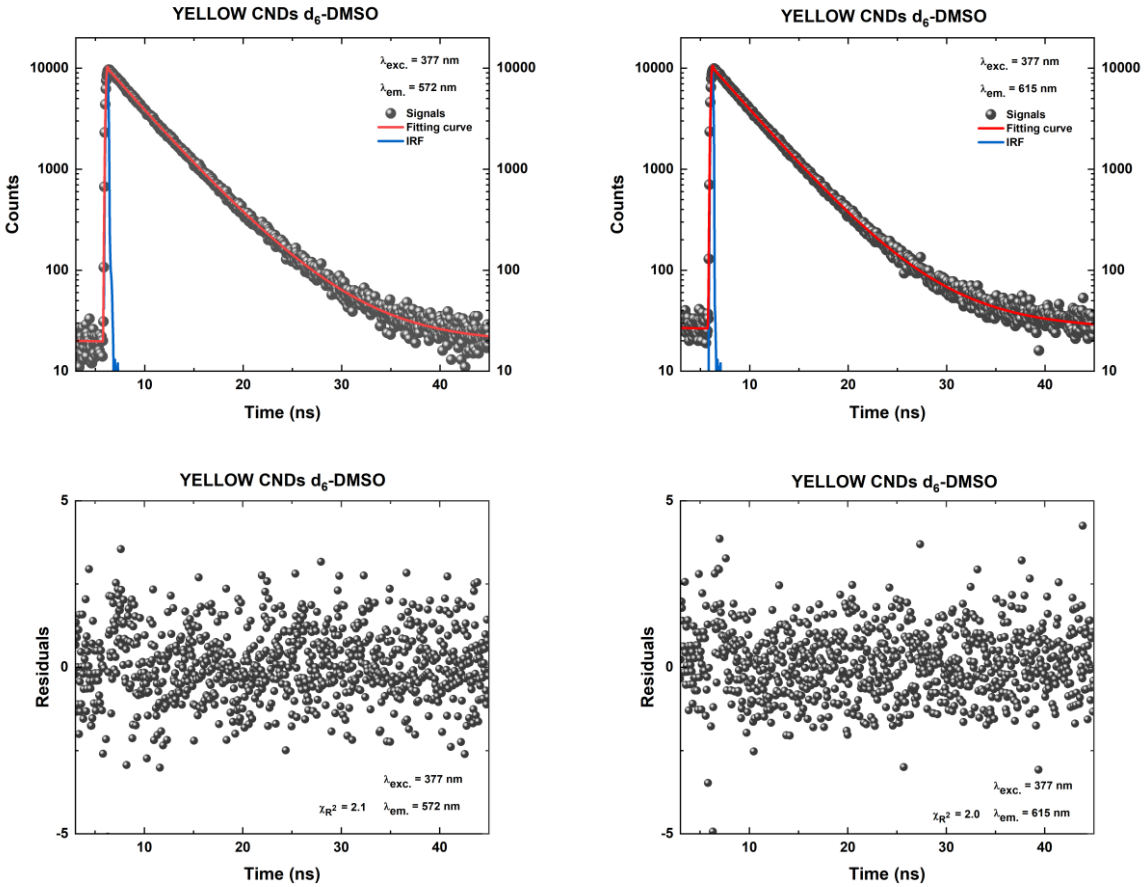

Figure S32. The fluorescence decay profiles of YELLOW CNDs in d_6-DMSO and their residual plots recorded at 572 nm and 615 nm, respectively.

Table S7. The fluorescence dynamics characteristics: fluorescence lifetimes, the standard deviations, and the contribution (in the bracket).

Type	Solvent	Fluorescence lifetimes (ns)		
		τ_1	τ_2	<τ>
CYAN	methanol	478 nm: **3.925±0.004** (100%) 511 nm: **3.929±0.004** (100%)	-	478 nm: **3.925±0.004**[a] 511 nm: **3.929±0.004**[a]
GREEN		509 nm: **3.206±0.164** (100%) 544 nm: **3.306±0.057** (100%)	-	509 nm: **3.206±0.164**[a] 544 nm: **3.306±0.057**[a]
YELLOW		552 nm: **2.801±0.002** (100%) 594 nm: **2.810±0.002** (100%)	-	552 nm: **2.801±0.002**[a] 594 nm: **2.810±0.002**[a]
YELLOW	d_6-DMSO	572 nm: **3.995±0.040** (94.6%) 615 nm: **3.994±0.051** (97.2%)	572 nm: **8.573±1.710** (5.4%) 615 nm: **9.45±1.648** (2.8%)	572 nm: **4.409±0.130** 615 nm: **4.283±0.095**

[a] Since methanol dispersions of PG CNDs provide the mono-exponential decays, there is only one lifetime component and no need to estimate the averaged value.

Table S8. The fluorescence dynamics characteristics: rate constants and the error values (in the bracket).

Type	Solvent	Radiative rate constant (ns^{-1})	Non-radiative rate constant (ns^{-1})
CYAN	methanol	478 nm: **0.158±0.001** 511 nm: **0.157±0.001**	478 nm: **0.0973±0.0008** 511 nm: **0.0972±0.0009**
GREEN		509 nm: **0.0928±0.0048** 544 nm: **0.0900±0.0016**	509 nm: **0.219±0.017** 544 nm: **0.213±0.005**
YELLOW		552 nm: **0.0901±0.0001** 594 nm: **0.0898±0.0001**	552 nm: **0.2669±0.0003** 594 nm: **0.2660±0.0003**
YELLOW	d_6-DMSO	572 nm: **0.102±0.003** 615 nm: **0.105±0.002**	572 nm: **0.125±0.007** 615 nm: **0.129±0.006**

One-photon fluorescence characteristics of PG CNDs: thermal decomposition *vs.* solvothermal treatment

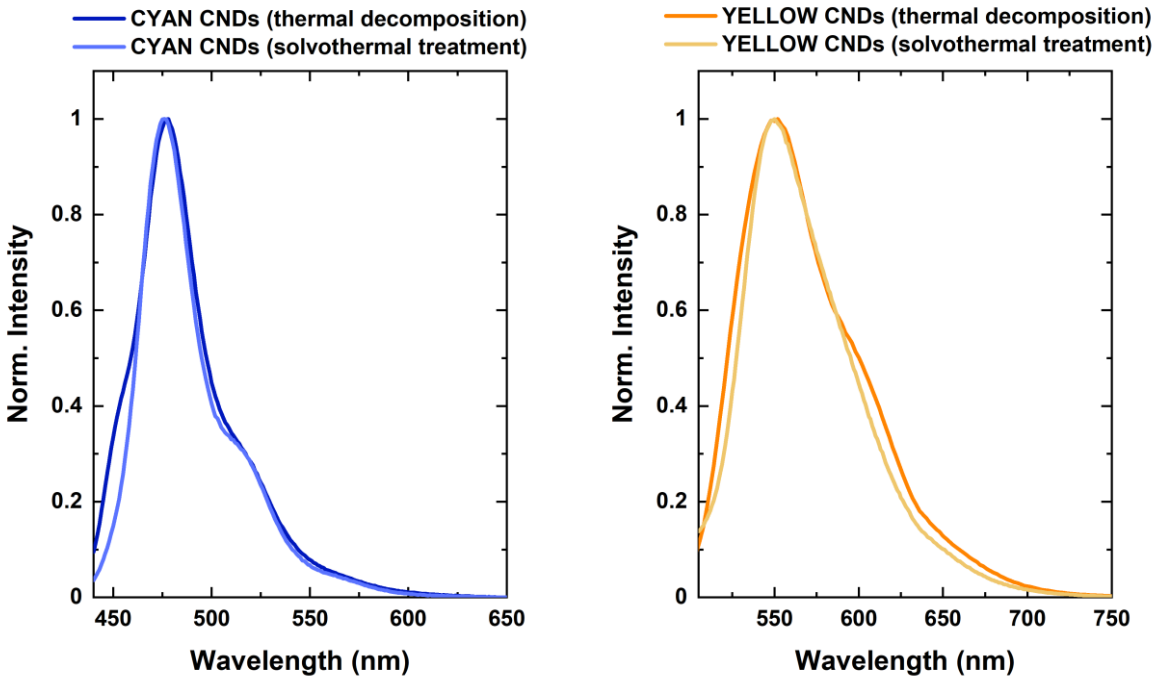

Figure S33. The comparison of normalized OPEF spectra of **CYAN** CNDs and **YELLOW** CNDs derived from different synthesis routes (the thermal decomposition and the solvothermal treatment).

Power-dependence multiphoton assays

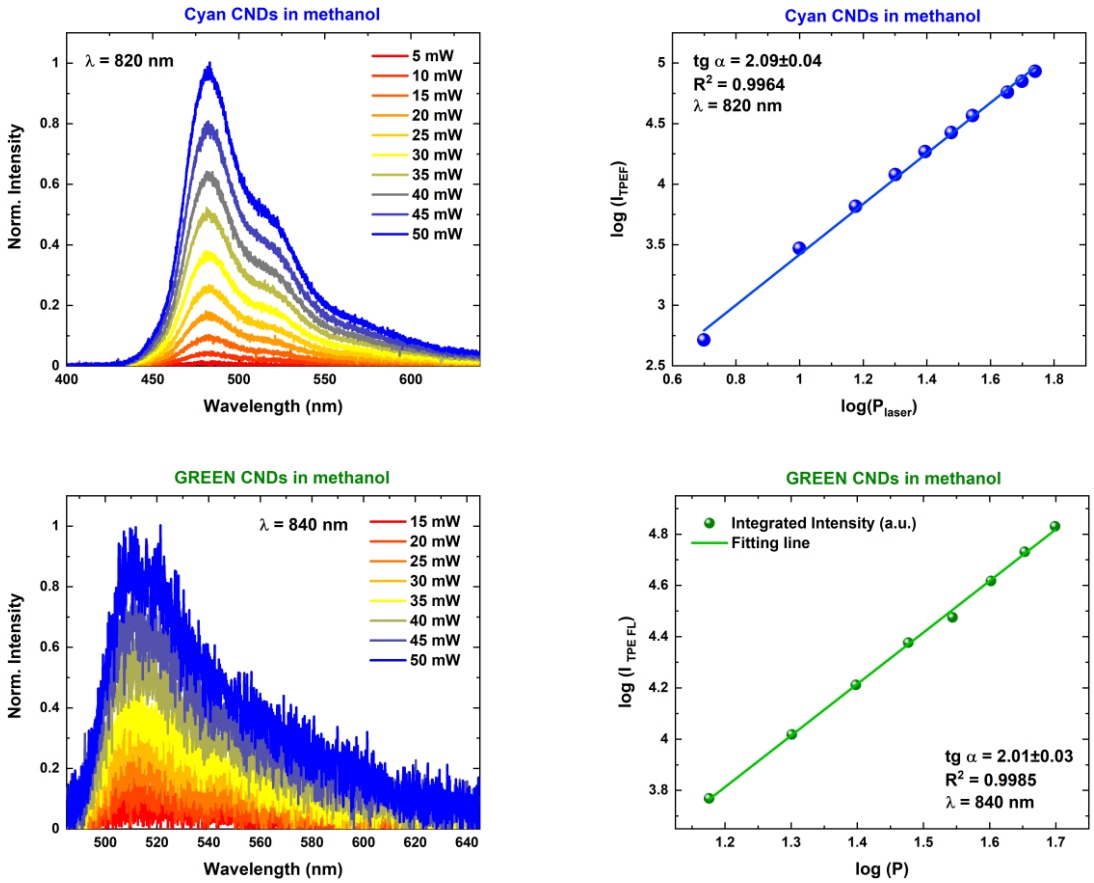

Figure S34. The evolution of the TPEF spectra of **CYAN** and **GREEN** CNDs in methanol *vs.* the excitation laser power.

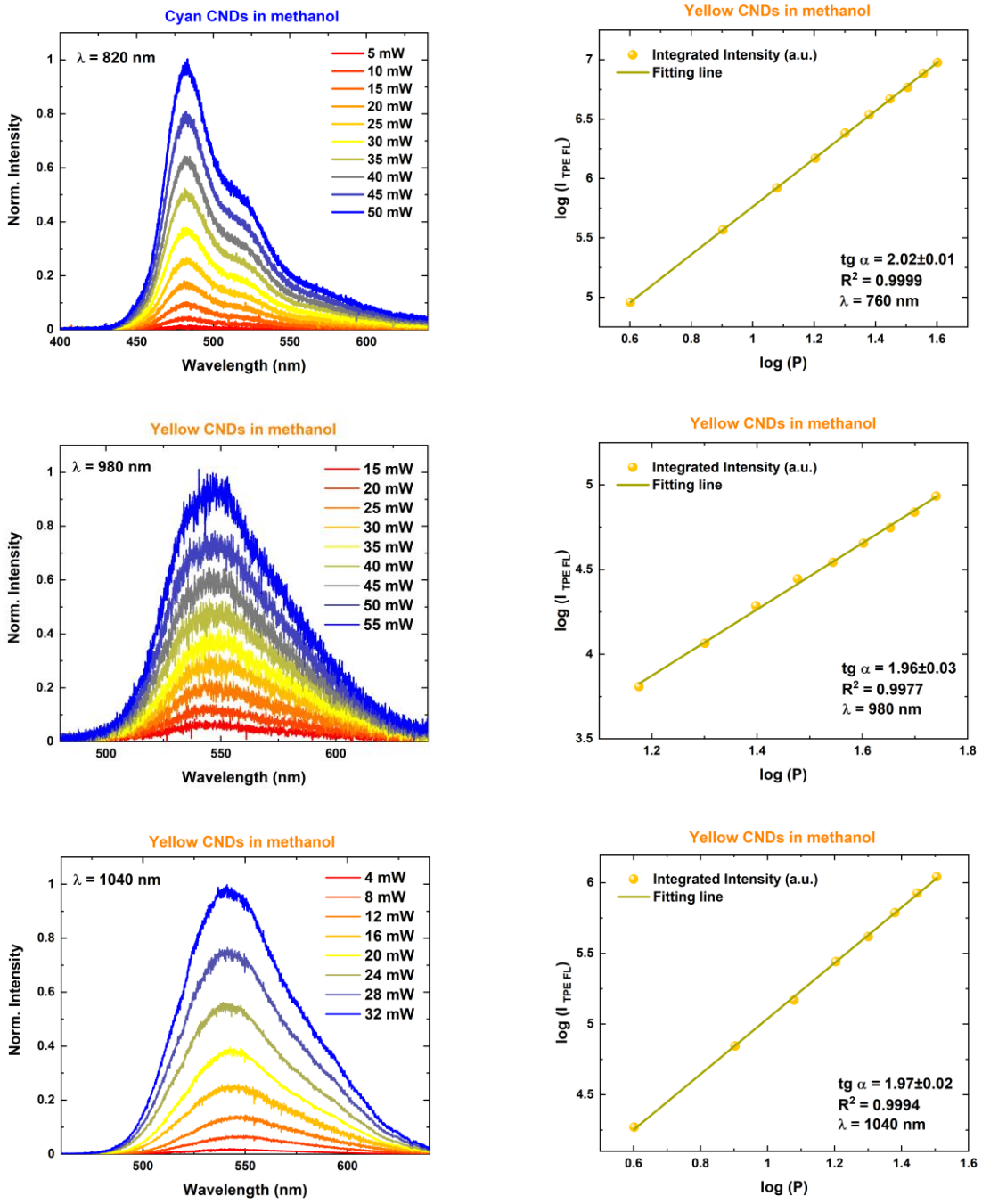

Figure S35. The evolution of the TPEF spectra of **YELLOW** CNDs in methanol *vs.* the excitation laser power.

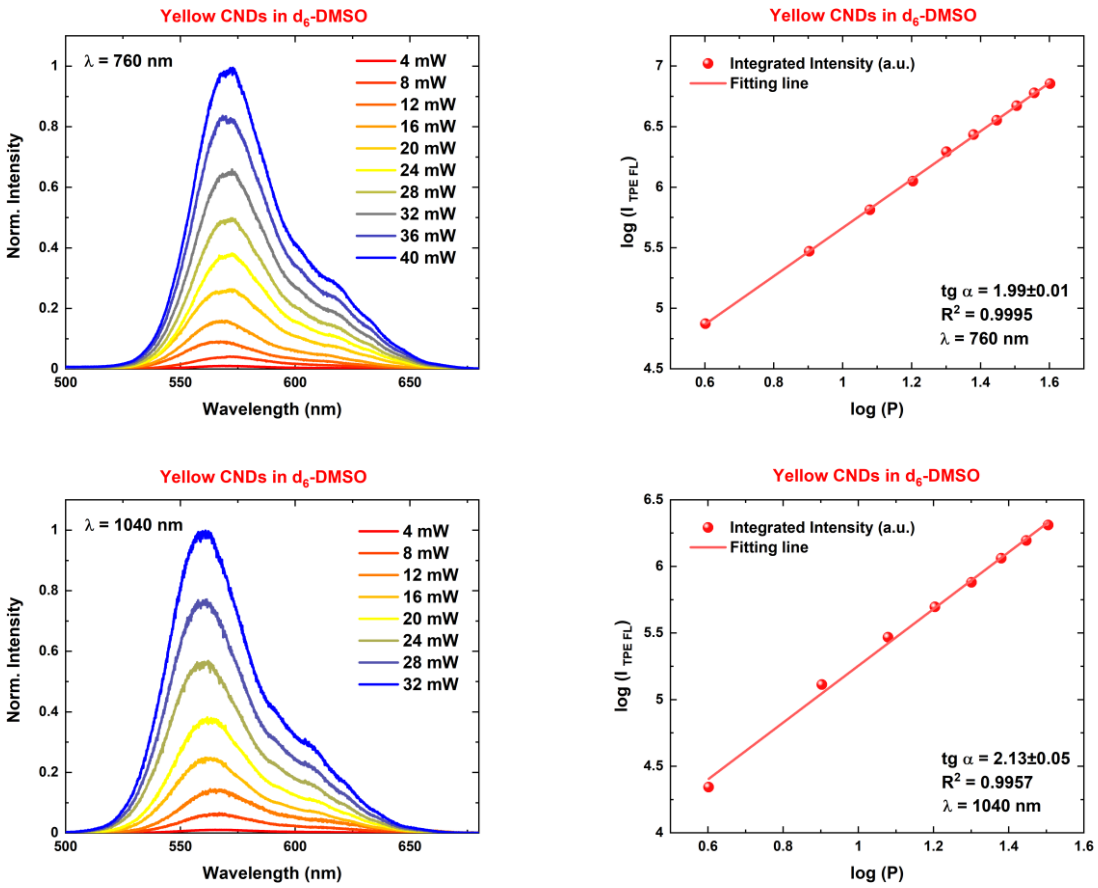

Figure S36. The evolution of the TPEF spectra of **YELLOW** CNDs in d_6-DMSO *vs.* the excitation laser power.

Two-photon excitation-emission maps

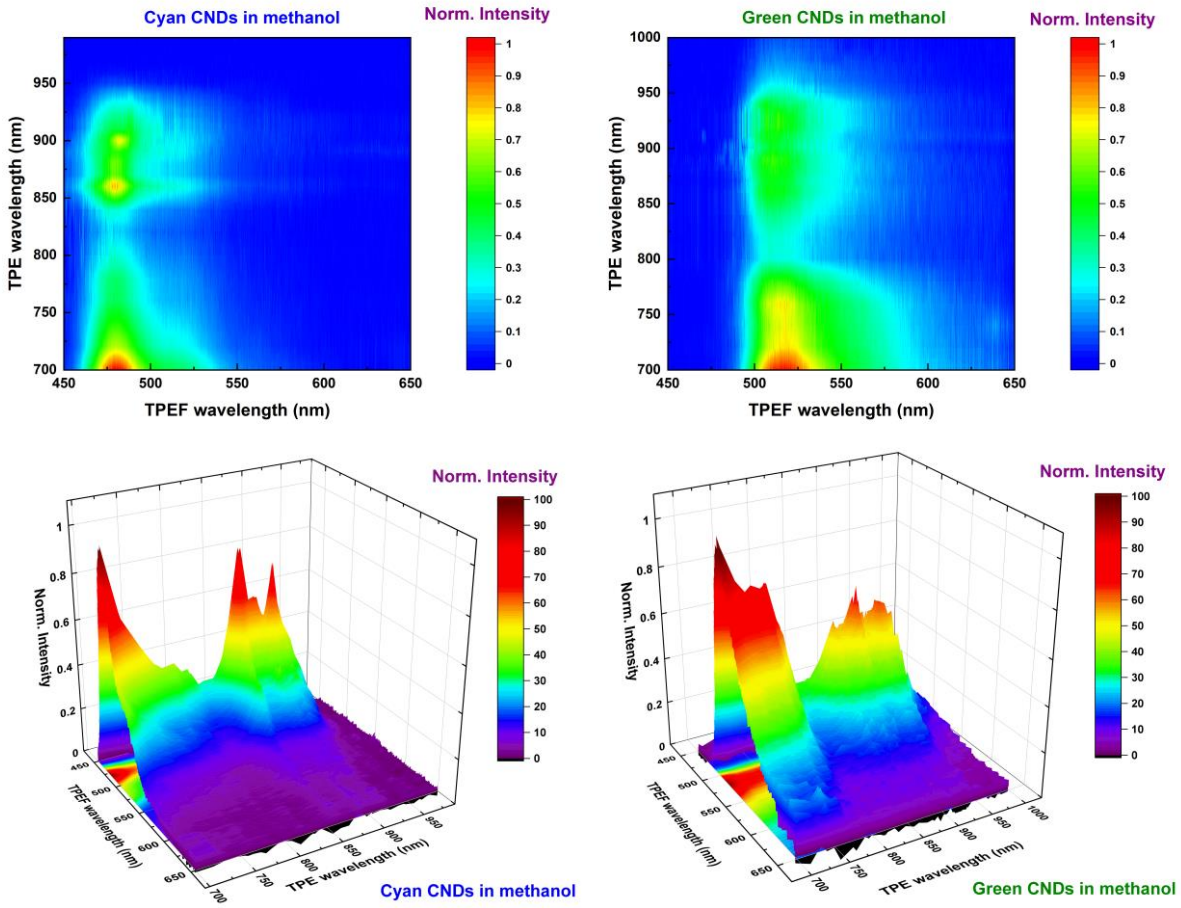

Figure S37. The two-photon excitation-emission maps and three-dimensional spectra of **CYAN** and **GREEN** CNDs in methanol dispersions.

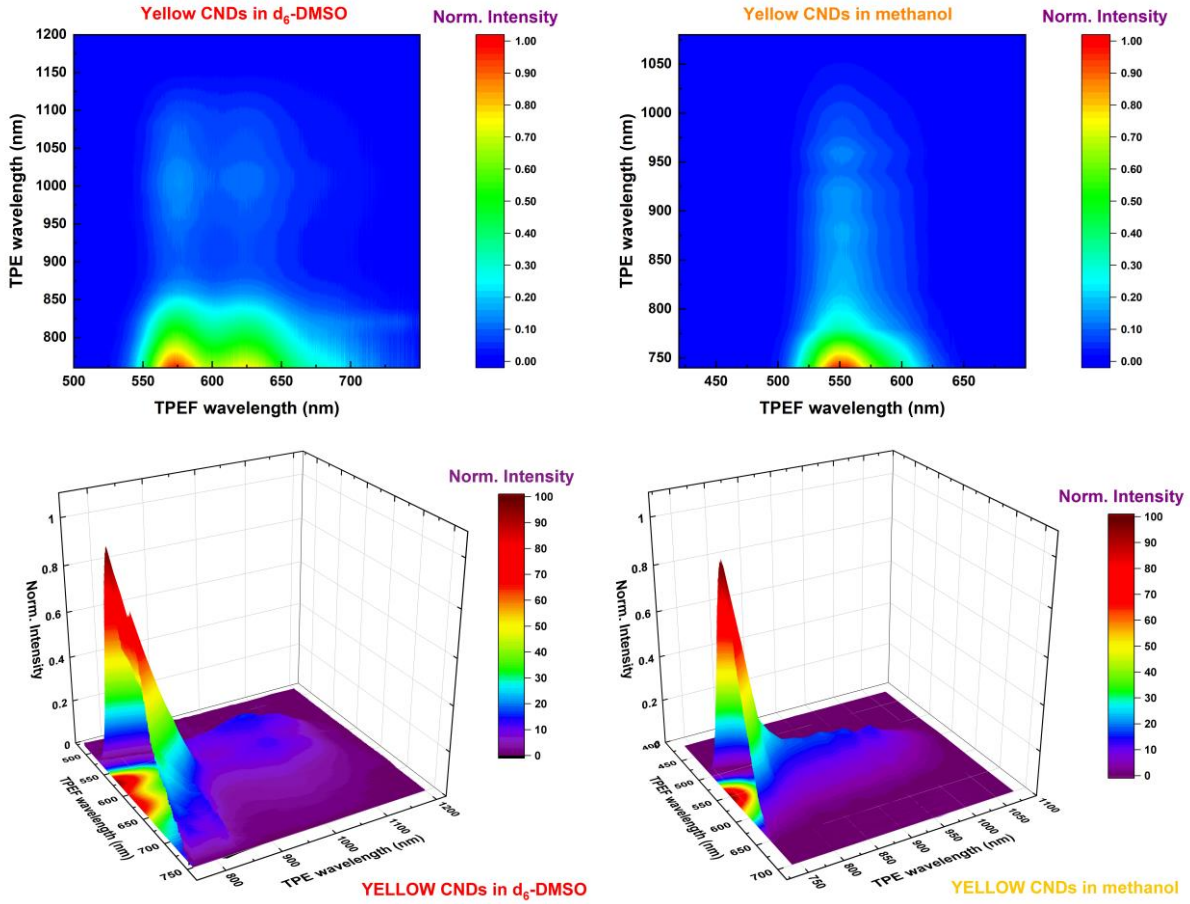

Figure S38. The two-photon excitation-emission maps and three-dimensional spectra of YELLOW CNDs in d_6-DMSO and methanol dispersions.

Two-photon absorption cross-section and two-photon brightness

To quantify the TPA and TPEF properties, the TPA cross-sections of PG CNDs can be estimated from the luminescence method, following the formula:

$$\sigma_{TPA,\,s} = \sigma_{TPA,\,r}\frac{I_s C_r \varphi_r n_s}{I_r C_s \varphi_s n_r} \quad \textit{(equation 8)}$$

where σ_{TPA} stands for the TPA cross-section (GM); **I** is the integrated TPEF intensity (a.u.); **n** and **ϕ** denote the refractive index of the solvent and the FQY, respectively; **C** denotes the molar concentration. Subscripts **r** and **s** indicate reference and sample, respectively.[5-9]

The relevant fluorescent dyes were used as references: fluorescein in aqueous basic medium (for **CYAN** and **GREEN** CNDs in methanol), rhodamine 6G in methanol (for **YELLOW** CNDs in methanol), and rhodamine B in methanol (for **YELLOW** CNDs in d_6-DMSO).

To provide the reliable σ_{TPA} performance, the σ_{TPA} values of PG CNDs were also normalized with the molar mass value, as follows:

$$\sigma_{TPA,\ norm.} = \frac{\sigma_{TPA,\,s}}{M} \quad \textit{(equation 9)}$$

where $\sigma_{TPA,\,norm}$ stands for the normalized TPA cross-section (GM); **M** is the molar mass of PG CNDs;

The two-photon brightness parameters were calculated by multiplying σ_{TPA} and FQY values.

Two-photon absorption cross-section: reference dyes

Table S9. Two-photon absorption cross-sections of reference dyes: Fluorescein (for **CYAN** and **GREEN** CNDs in methanol), Rhodamine 6G (for **YELLOW** CNDs in methanol), and Rhodamine B (for **YELLOW** CNDs in d_6-DMSO).[6]

Laser wavelength (nm)	Two-photon absorption cross-section (GM)	Laser wavelength (nm)	Two-photon absorption cross-section (GM)	
	Fluorescein in basic medium		Rhodamine 6G in methanol	Rhodamine B in methanol
700	14	700	-	-
720	21	720	-	-
740	30	740	53	-
760	45	760	55	72
780	45	780	56	95
800	36	800	65	120
820	28	820	64	300
840	13	840	42	180
860	12	860	12	110
870	12	880	4.4	54
880	12	900	4.2	13
890	14	920	5.7	6.0
900	15	940	8.3	7.7
910	16	960	11	11
920	16	980	13	14
930	14	1000	9.5	22
940	11	1020	7.1	34
950	8.0	1040	8.3	39
960	6.3	1060	9.9	31
970	5.7	1080	7.0	24
980	5.2	1100	-	24
990	4.2	1150	-	2.6
1000	2.7	1200	-	0.19

Two-photon absorption cross-section: PG CNDs

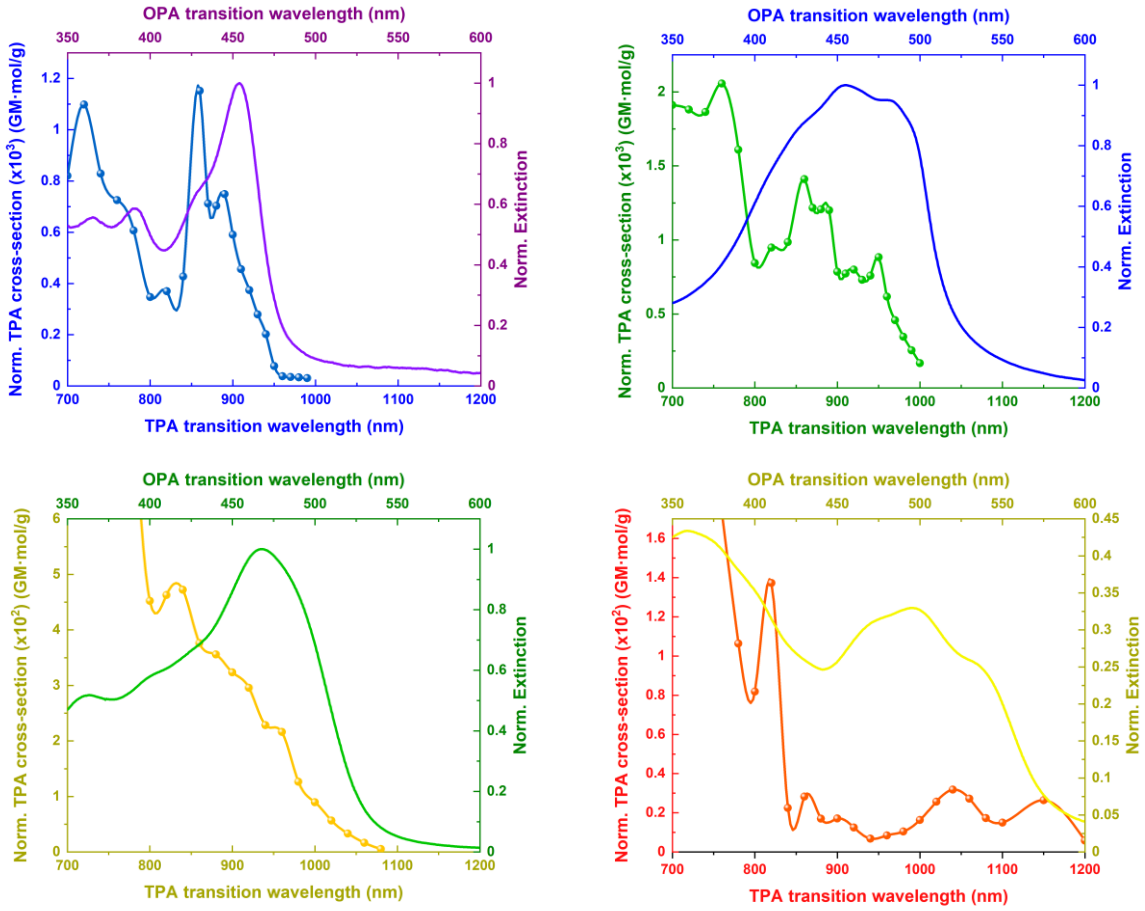

Figure S39. The normalized UV-Vis extinction and TPA spectra of individual PG CNDs: a) **CYAN** CNDs in methanol b) **GREEN** CNDs in methanol, c) **YELLOW** CNDs in methanol, and d) **YELLOW** CNDs in d_6-DMSO. Each spectrum is described by relevant x- and y-axes with the same colour.

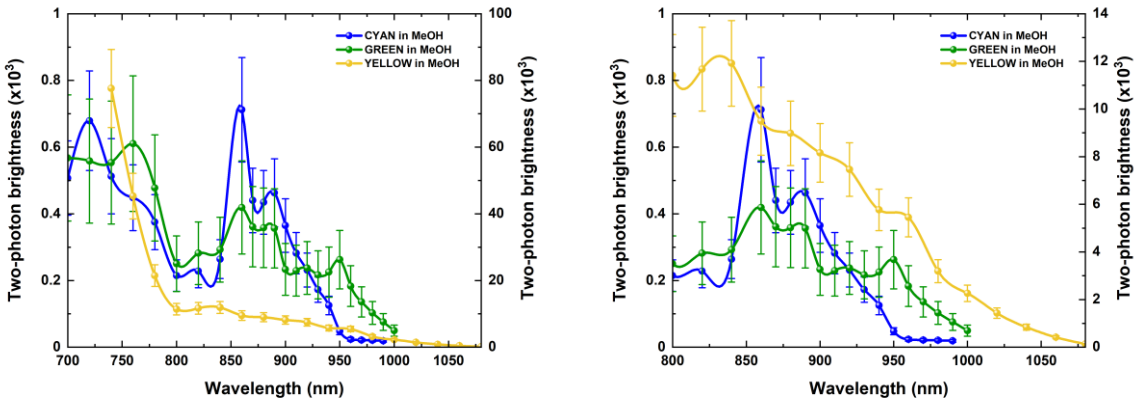

Figure S40. The normalized two-photon brigthness spectra of PG CNDs. The brightness values of **CYAN** and **GREEN** correspond to left y-axes while the right y-axes describe the two-photon brightness of **YELLOW** CNDs.

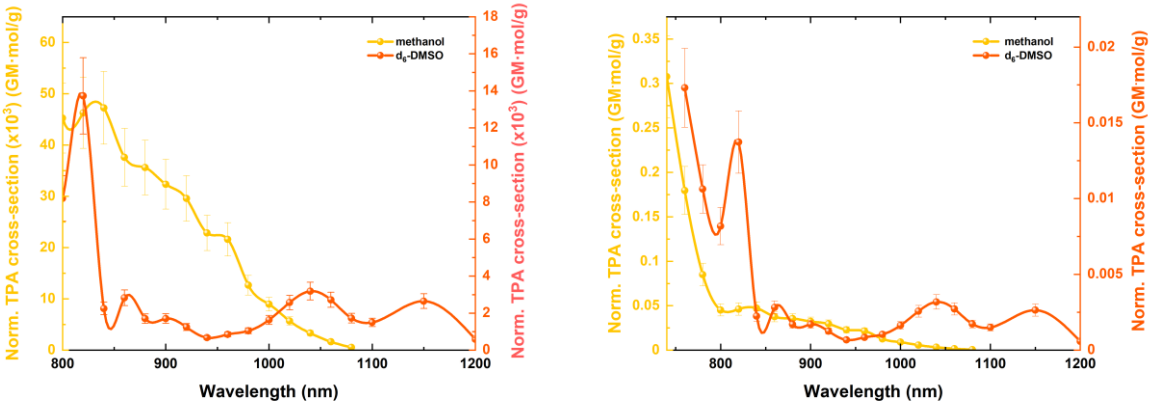

Figure S41. The normalized TPA spectra of **YELLOW** CNDs dispersed in methanol and d_6-DMSO in full and narrower windows. The curve colour indicates a proper y-axis.

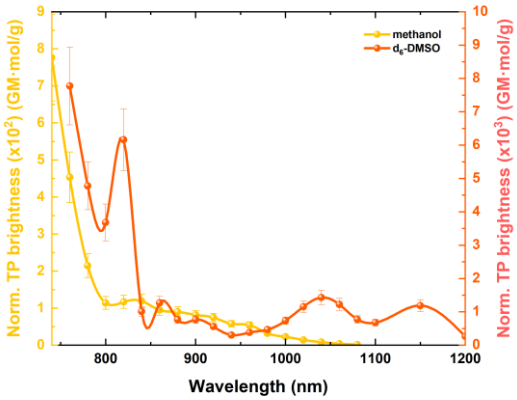

Figure S42. The normalized two-photon brightness spectra of **YELLOW** CNDs dispersed in methanol and d_6-DMSO in the full window. The curve colour indicates a proper y-axis.

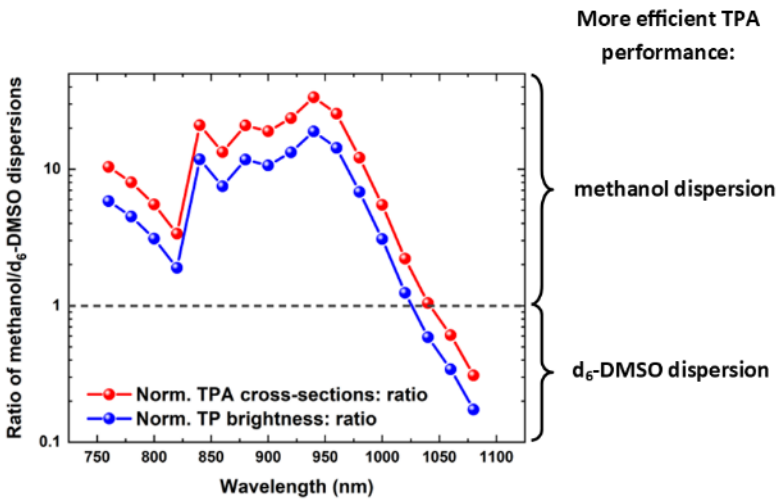

Figure S43. The ratio of the two-photon absorption cross-section and two-photon brightness of YELLOW CNDs in methanol and d_6-DMSO dispersion in the common wavelength range. The ratios were calculated as follows: the parameter of the methanol sample was divided by the d_6-DMSO suspension parameter. The more efficient two-photon absorbing suspension was indicated on the right side of the graph.

Hansen Solubility Parameters

The Hansen Solubility Parameter (δ) describes the similarity between solvating media and the solute, considering the interactions which can be involved between them: *like dissolves like*. Hence, the δ can be spread on three components which are associated with the energy from the hydrogen bonding ($\delta_{H.B.}$), the dispersion forces ($\delta_{Disper.}$), and dipolar intermolecular forces ($\delta_{Polar.}$), as follows:

$$\boldsymbol{\delta^2 = \delta^2_{H.B.} + \delta^2_{Disper.} + \delta^2_{Polar.}} \quad \textit{(equation 10)}$$

where all **δ**, $\boldsymbol{\delta_{H.B.}}$, $\boldsymbol{\delta_{Disper.}}$ and $\boldsymbol{\delta_{Polar.}}$ components are described above (MPa$^{0.5}$; see **Table S9**).[10-11]

Kamlet-Taft solvatochromic parameters

To quantify the ability of the solvent to interact with the solute, the linear solvation energy equation was also used:

$$\boldsymbol{XYZ = XYZ_0 + s(\pi^* + d\delta) + a\alpha + b\beta + h\delta_H + e\xi} \quad \textit{(equation 11)}$$

where **XYZ** and $\boldsymbol{XYZ_0}$ are general terms corresponding to different chemical/physical properties in varying and initial conditions, respectively; **π*** denotes the index of the solvent polarizability; **δ** is the *polarizability correction term*; **α** and **β** are the hydrogen bonding acidity and basicity parameters, respectively; $\boldsymbol{\delta_H}$ is the Hildebrand Solubility Parameter; **ξ** is the *coordinate covalency* parameter; **s**, **d**, **a**, **b**, **h**, and **e** are regression coefficients for given system.[12]

Among them, α and β are considered to be crucial in the characterization of the role of the solvent in the formation of the hydrogen bonding network with the solute (**Table S9**).

Reichardt's Scale of solvent polarity

The solvent polarity can be also expressed using the so-called Reichardt's scale parameter (E_T (30)) or its normalized version (E_T(N)) which corresponds to the molar electronic transition energy, determined for pyridinium N-phenolate betaine dye dissolved in the variety of solvents (see **Table S9**).[13]

Table S10. The solvents' characteristics.[12-14]

No.	Name	δ^{a} ($MPa^{0.5}$)	$\delta_{H.B.}$ ($MPa^{0.5}$)	$\delta_{Disper.}$ ($MPa^{0.5}$)	$\delta_{Polar.}$ ($MPa^{0.5}$)	α	β	π*	$E_T(30)$ (kcal/mol)	$E_T(N)$ (kcal/mol)
1	Ethylene glycol	33.0	26.0	17.0	11.0	0.90	0.52	0.92	56.3	0.79
2	Methanol	29.6[b]	22.3[b]	15.1[b]	12.3[b]	0.93[b]	0.62[b]	0.60[b]	55.4[b]	0.762[b]
3	Deuterated methanol	29.6[b]	22.3[b]	15.1[b]	12.3[b]	0.93[b]	0.62[b]	0.60[b]	55.4[b]	0.762[b]
4	Ethanol	26.5	19.4	15.8	8.8	0.83	0.77	0.54	51.9	0.654
5	Isopropanol	23.6	16.4	15.8	6.1	0.76	0.95	0.48	48.4	0.546
6	n-butanol	23.2	15.8	16.0	5.7	0.79	0.88	0.47	49.7	0.586
7	n-pentanol	21.9	13.9	15.9	5.9	0.84[c]	0.86[c]	0.40[c]	49.1	0.586
8	Cyclohexanol	22.4	13.5	17.4	4.1	0.66[c]	0.84[c]	0.45[c]	47.2	0.509
9	n-heptanol	20.5	11.7	16.0	5.3	0.80	0.83	0.58	48.5	0.549
10	DMF	24.9	11.3	17.4	13.7	0.00	0.69	0.88	43.2	0.386
11	Deuterated DMSO	26.7[b]	10.2[b]	18.4[b]	16.4[b]	0.00[b]	0.76[b]	1.00[b]	45.1[b]	0.444[b]
12	DMSO	26.7[b]	10.2[b]	18.4[b]	16.4[b]	0.00[b]	0.76[b]	1.00[b]	45.1[b]	0.444[b]
13	Acetone	19.9	7.0	15.5	10.4	0.08	0.48	0.71	42.2	0.355

[a] The overall δ parameter was calculated by combining its components in the above-mentioned equation.

[b] Deuterated methanol and DMSO are assumed to be described by the same δ and α parameters as their hydrogen-including analogues.

[C] Parameters were found on http://www.stenutz.eu/chem/solv26.php [available on August 6th 2023].

One-photon excited fluorescence *vs.* solvent effect

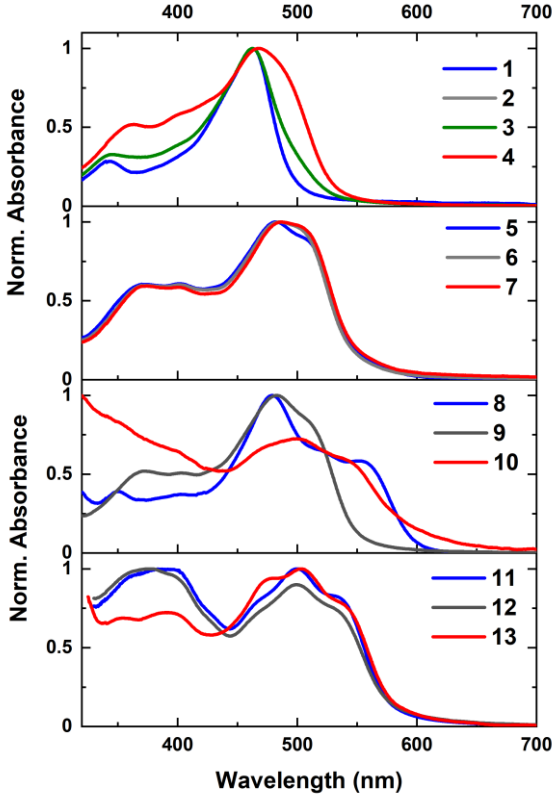

Figure S44. The UV-Vis extinction spectra of YELLOW CNDs dispersed in different media. Each solvent is numbered as follows: 1 - ethylene glycol, 2 – methanol, 3 - d_4-methanol, 4 - ethanol, 5 – isopropanol, 6 – n-butanol, 7 – n-pentanol, 8 – cyclohexanol, 9 – n-heptanol, 10 – dimethylformamide (DMF), 11 – d_6-DMSO, 12 – DMSO, and 13 – acetone.

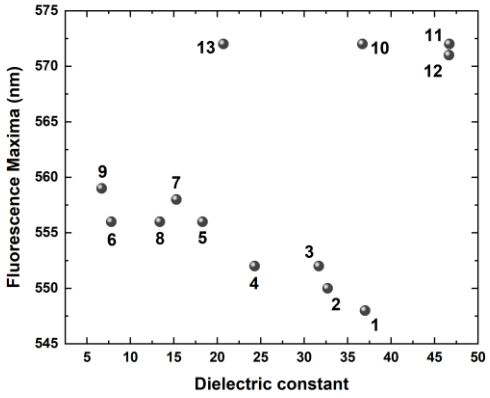

Figure S45. The OPEF maxima of YELLOW CNDs plotted *vs.* the relative permittivity of their corresponding solvents. Each solvent is numbered as follows: 1 - ethylene glycol, 2 – methanol, 3 - d_4-methanol, 4 - ethanol, 5 – isopropanol, 6 – n-butanol, 7 – n-pentanol, 8 – cyclohexanol, 9 – n-heptanol, 10 – DMF, 11 – d_6-DMSO, 12 – DMSO, and 13 – acetone.

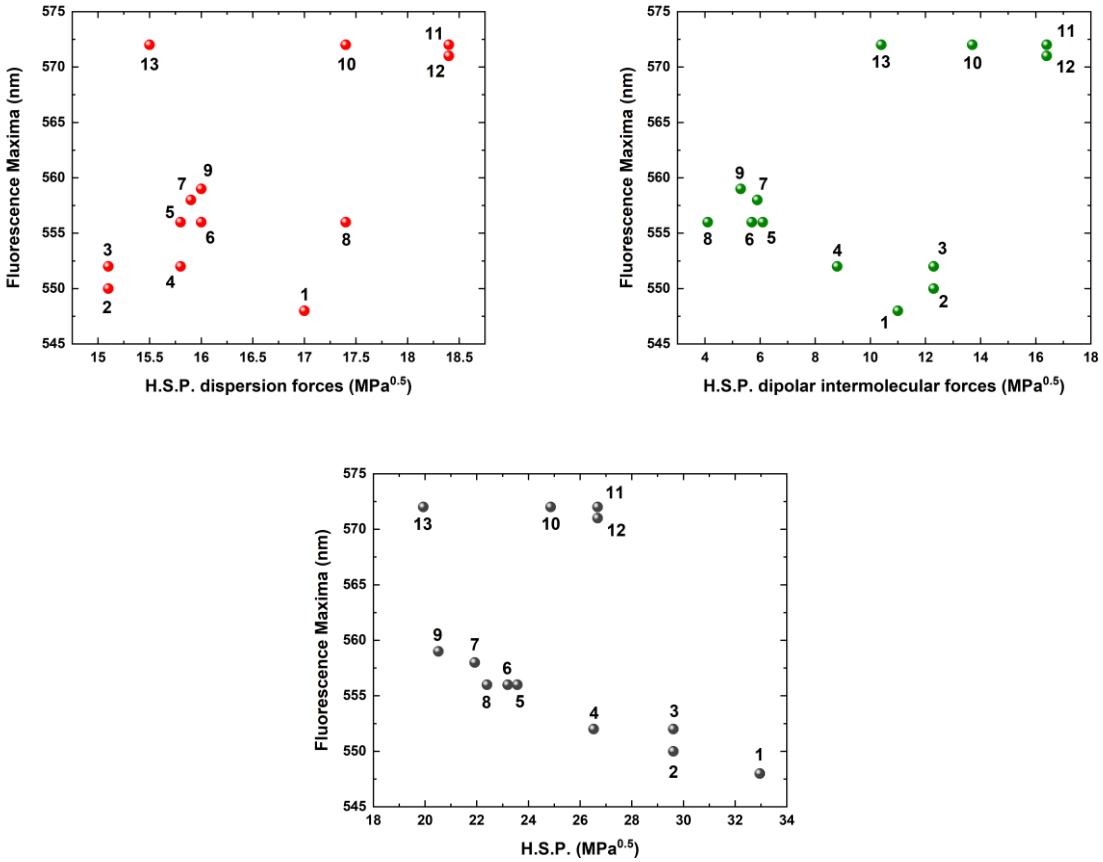

Figure S46. The correlation between the OPEF maxima of YELLOW CNDs and Hansen Solubility Parameters of their corresponding solvents. Each solvent is numbered as follows: 1 - ethylene glycol, 2 – methanol, 3 - d_4-methanol, 4 - ethanol, 5 – isopropanol, 6 – n-butanol, 7 – n-pentanol, 8 – cyclohexanol, 9 – n-heptanol, 10 – DMF, 11 – d_6-DMSO, 12 – DMSO, and 13 – acetone.

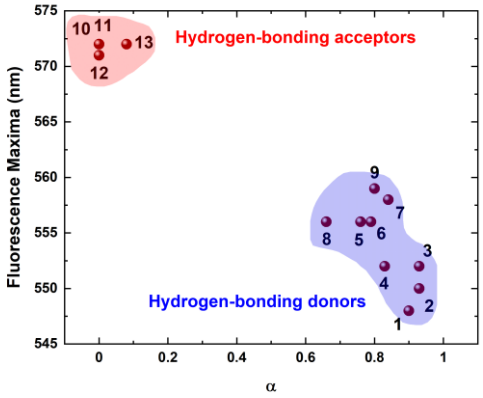

Figure S47. The correlation between the OPEF maxima of **YELLOW** CNDs and the Kamlet-Taft solvatochromic parameters. Each solvent is numbered as follows: 1 - ethylene glycol, 2 – methanol, 3 - d_4-methanol, 4 - ethanol, 5 – isopropanol, 6 – n-butanol, 7 – n-pentanol, 8 – cyclohexanol, 9 – n-heptanol, 10 – DMF, 11 – d_6-DMSO, 12 – DMSO, and 13 – acetone.

Temperature-dependent one-photon excited fluorescence

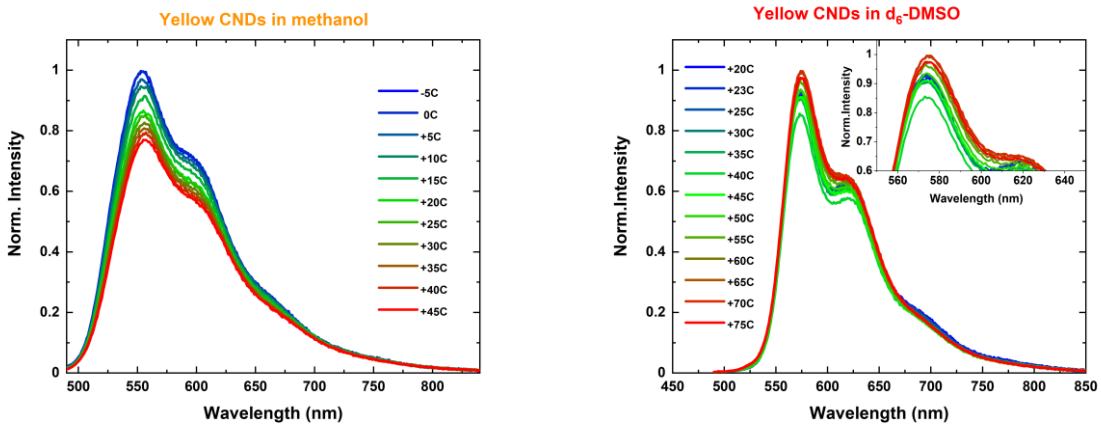

Figure S48. The evolution of OPEF spectra recorded for varying temperatures ($\lambda_{exc.}$ = 460 nm). The different curve colours correspond to changing temperature values.

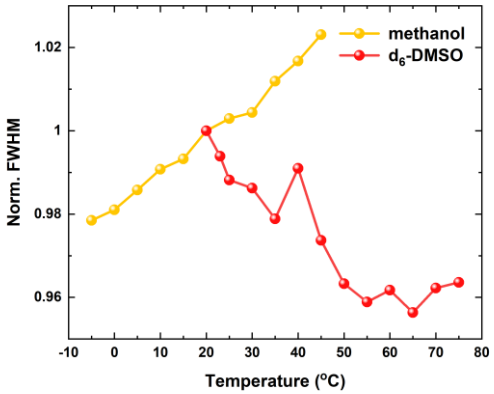

Figure S49. The evolution of the FWHM values of the OPEF spectra of YELLOW CNDs. Each FWHM parameter was normalized with the respect to the relevant FWHM value at 20°C.

Temperature-dependent extinction spectra

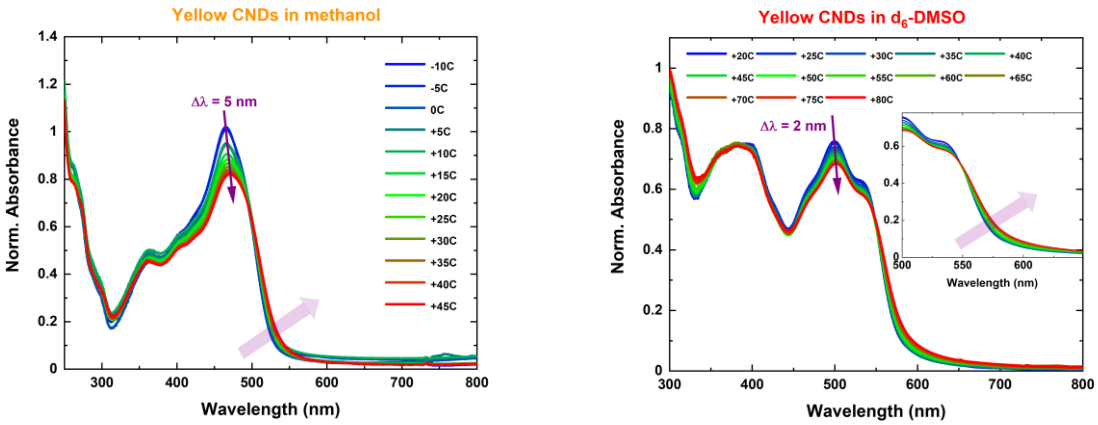

Figure S50. The evolution of the absorption peaks of **YELLOW** CNDs in methanol and d_6-DMSO as a function of the applied temperature. The narrow violet arrows indicate the red shifts of the major peak while the bold arrows show the spectral shift direction of the whole absorption spectra.

References:

1. Highet, R. J.; Chou, F.-T. E., The dependence of phenol-dienone tautomerism upon the hydrogen bonding characteristics of the solvent: 3,5-dipyrrolidinophenol. *Journal of the American Chemical Society* **1977,** *99* (10), 3538-3539.
2. Highet, R. J.; Ekhato, I. V., Keto-enol tautomerism of phloroglucinol and the formation of the tris(sodium bisulfite) addition complex. *The Journal of Organic Chemistry* **1988,** *53* (12), 2843-2844.
3. Tauc, J.; Menth, A., States in the gap. *Journal of Non-Crystalline Solids* **1972,** *8-10*, 569-585.
4. Ferreyra, D. D.; Rodríguez Sartori, D.; Ezquerra Riega, S. D.; Rodríguez, H. B.; Gonzalez, M. C., Tuning the nitrogen content of carbon dots in carbon nitride nanoflakes. *Carbon* **2020,** *167*, 230-243.
5. Medishetty, R.; Zaręba, J. K.; Mayer, D.; Samoć, M.; Fischer, R. A., Nonlinear optical properties, upconversion and lasing in metal–organic frameworks. *Chemical Society Reviews* **2017,** *46* (16), 4976-5004.
6. Makarov, N. S.; Drobizhev, M.; Rebane, A., Two-photon absorption standards in the 550–1600 nm excitation wavelength range. *Opt. Express* **2008,** *16* (6), 4029-4047.
7. Samoc, M.; Matczyszyn, K.; Nyk, M.; Olesiak-Banska, J.; Wawrzynczyk, D.; Hanczyc, P.; Szeremeta, J.; Wielgus, M.; Gordel, M.; Mazur, L.; Kolkowski, R.; Straszak, B.; Cifuentes, M.; Humphrey, M., *Nonlinear absorption and nonlinear refraction: maximizing the merit factors*. SPIE: 2012; Vol. 8258.
8. Schwich, T.; Cifuentes, M. P.; Gugger, P. A.; Samoc, M.; Humphrey, M. G., Electronic, Molecular Weight, Molecular Volume, and Financial Cost-Scaling and Comparison of Two-Photon Absorption Efficiency in Disparate Molecules (Organometallic Complexes for Nonlinear Optics. 48.) – A Response to "Comment on 'Organometallic Complexes for Nonlinear Optics. 45. Dispersion of the Third-Order Nonlinear Optical Properties of Triphenylamine-Cored Alkynylruthenium Dendrimers.' Increasing the Nonlinear Response by Two Orders of Magnitude.". *Advanced Materials* **2011,** *23* (12), 1433-1435.
9. Roberts, R. L.; Schwich, T.; Corkery, T. C.; Cifuentes, M. P.; Green, K. A.; Farmer, J. D.; Low, P. J.; Marder, T. B.; Samoc, M.; Humphrey, M. G., Organometallic Complexes for Nonlinear Optics. 45. Dispersion of the Third-Order Nonlinear Optical Properties of Triphenylamine-Cored Alkynylruthenium Dendrimers. *Advanced Materials* **2009,** *21* (22), 2318-2322.
10. Hansen, C. M., The three dimensional solubility parameter. *Danish Technical: Copenhagen* **1967,** *14*.
11. Hansen, C. M., *Hansen Solubility Parameters: A User's Handbook, Second Edition*. CRC Press: 2007.
12. Kamlet, M. J.; Abboud, J. L. M.; Abraham, M. H.; Taft, R. W., Linear solvation energy relationships. 23. A comprehensive collection of the solvatochromic parameters, .pi.*, .alpha., and .beta., and some methods for simplifying the generalized solvatochromic equation. *The Journal of Organic Chemistry* **1983,** *48* (17), 2877-2887.
13. Reichardt, C., Solvatochromic Dyes as Solvent Polarity Indicators. *Chemical Reviews* **1994,** *94* (8), 2319-2358.
14. Lan, Y.; Corradini, M. G.; Liu, X.; May, T. E.; Borondics, F.; Weiss, R. G.; Rogers, M. A., Comparing and correlating solubility parameters governing the self-assembly of molecular gels using 1,3:2,4-dibenzylidene sorbitol as the gelator. *Langmuir* **2014,** *30* (47), 14128-42.